Thermodynamics of atomic and ionized hydrogen: Analytical results versus equation-of-state tables and Monte Carlo data

A. Alastuey
Laboratoire de Physique, ENS Lyon, UMR CNRS 5672, 46 allée d'Italie, 69364 Lyon Cedex 07, France

V. Ballenegger
Institut UTINAM, Université de Franche-Comté, UMR CNRS 6213, 16, route de Gray, 25030 Besançon cedex France

(Received 8 August 2012; published 6 December 2012)

We compute thermodynamical properties of a low-density hydrogen gas within the physical picture, in which the system is described as a quantum electron-proton plasma interacting via the Coulomb potential. Our calculations are done using the exact scaled low-temperature (SLT) expansion, which provides a rigorous extension of the well-known virial expansion—valid in the fully ionized phase—into the Saha regime where the system is partially or fully recombined into hydrogen atoms. After recalling the SLT expansion of the pressure [A. Alastuey *et al.*, J. Stat. Phys. **130**, 1119 (2008)], we obtain the SLT expansions of the chemical potential and of the internal energy, up to order $\exp(-|E_H|/kT)$ included ($E_H \simeq -13.6$ eV). Those truncated expansions describe the first five nonideal corrections to the ideal Saha law. They account exactly, up to the considered order, for all effects of interactions and thermal excitations, including the formation of bound states (atom H, ions H^- and H_2^+, molecule H_2, ...) and atom-charge and atom-atom interactions. Among the five leading corrections, three are easy to evaluate, while the remaining ones involve well-defined internal partition functions for the molecule H_2 and ions H^- and H_2^+, for which no closed-form analytical formula exist currently. We provide accurate low-temperature approximations for those partition functions by using known values of rotational and vibrational energies. We compare then the predictions of the SLT expansion, for the pressure and the internal energy, with, on the one hand, the equation-of-state tables obtained within the opacity program at Livermore (OPAL) and, on the other hand, data of path integral quantum Monte Carlo (PIMC) simulations. In general, a good agreement is found. At low densities, the simple analytical SLT formulas reproduce the values of the OPAL tables up to the last digit in a large range of temperatures, while at higher densities ($\rho \sim 10^{-2}$ g/cm^3), some discrepancies among the SLT, OPAL, and PIMC results are observed.

DOI: 10.1103/PhysRevE.86.066402 PACS number(s): 52.25.Kn, 67.10.Fj

I. INTRODUCTION

As the lightest and most simple element, hydrogen is important both theoretically and for practical applications. It is also the most abundant element in the universe, and a precise knowledge of its thermodynamical properties is needed by astrophysicists over a wide range of pressures and temperatures. In that context, the derivation of accurate tables for thermodynamical functions is quite useful. This motivated the celebrated opacity program at Livermore (OPAL), which, in addition, provides tabulations of the opacity as a function of temperature and density, a key ingredient for astrophysical diagnosis.

The OPAL equation-of-state tables [1] have been derived from the activity expansion (ACTEX) method, first introduced in Ref. [2] and implemented through successive papers [3]. That approach is built within the physical picture, where hydrogen is described in terms of a quantum plasma made with protons and electrons interacting *via* the $1/r$ Coulomb potential. For a given set of thermodynamical parameters, one proceeds to suitable estimations of the expected relevant contributions in the activity expansions determined by simple physical arguments. This allows one to account for complex phenomena arising from the formation of chemical species and their interactions. The resulting OPAL tables are very reasonably accurate over a wide range of temperatures and densities, as checked through comparisons to quantum Monte Carlo simulations [4] and to high-pressure shock experiments [5].

Aside from the OPAL tables, exact asymptotic expansions can be used to provide reliable numerical data. It turns out that such an expansion, the so-called scaled low-temperature (SLT) expansion, has been recently derived in the Saha regime [6], where hydrogen reduces to a dilute partially ionized atomic gas. That regime is of particular astrophysical interest since it is observed, for instance, in the Sun interior. The main purpose of that paper is to derive, from the SLT expansion, simple and very precise estimations of the contributions of all the mechanisms at work in the Saha regime to any thermodynamical function. Our calculations avoid approximations introduced in the ACTEX approach, and they are written in terms of tractable analytic formulas which are quite easy to handle for determining the quantities of interest at any temperature and any density. No interpolation has to be performed as in other purely numerical tables like OPAL. The corresponding high-accuracy and thermodynamically consistent calculations should be quite useful for various applications, in particular the interpretation of recent seismology measurements in the Sun [7].

In the physical picture, the equation of state is studied by applying methods of quantum statistical mechanics to Coulombic matter. Various analytical methods have been developed for this purpose, such as effective potential methods [8–11], many-body perturbation theory [12,13], and Mayer diagrams in the polymer representation of the quantum system [14–16]. Numerical techniques have also been elaborated, in particular,

density functional theory molecular dynamics [17–19] and path-integral Monte Carlo (PIMC) simulations [20]. In the present work, we use a suitable extension [21]—needed for dealing with a partially recombined phase—of the quantum Mayer diagrams method introduced previously to derive in particular the virial expansion of the equation of state up to order $\rho^{5/2}$ in the density, both in the absence [14,22,23] and presence [24] of a magnetic field. This framework avoids the problems associated with the more widely used chemical approach [25–29] in which bound states (atoms H, molecules H_2, ions H^-, H_2^+, ...) are treated as preformed constituents that are assumed to interact via some given effective potentials [30,31] with the ionized charges and between themselves. The SLT expansion [6] solves the difficult problem of dealing consistently and exactly with screening and bound states in the Saha regime within the physical picture. Effect of atom-atom interactions and screened interactions between ionized charges and atoms appear, for instance, in our calculations, without introducing any intermediate modelization, as a consequence of the basic Coulombic interactions between the electrons and protons. They are embedded in functions $h_2(\beta)$ and $h_4(\beta)$ defined in Sec. II D. In the SLT expansion, the internal partition functions of all bound entities are finite thanks to a systematic account of collective screening effects. That expansion exhibits no missing term, nor double counting, for instance, between contributions associated to a hydrogen molecule or to two hydrogen atoms, despite the atoms may form a molecule at short distances.

The Saha regime corresponds to low-temperature and sufficiently low densities, so the most abundant chemical species are ionized protons, ionized electrons, and hydrogen atoms in their ground state. The corresponding thermal ionization equilibrium $H \rightleftarrows e + p$ is well described in first approximation by the mass-action law for ideal mixtures [32]

$$\frac{\rho_{\rm at}^{\rm id}}{\rho_p^{\rm id}\rho_e^{\rm id}} = \left(\frac{2\pi\hbar^2\beta}{m}\right)^{3/2} e^{-\beta E_{\rm H}}, \tag{1}$$

which relates the number density $\rho_{\rm at}^{\rm id}$ of hydrogen atoms in their ground state with energy $E_{\rm H} = -me^4/(2\hbar^2) \simeq -13.6\,{\rm eV}$ to the number densities $\rho_p^{\rm id}$ and $\rho_e^{\rm id}$ of ionized protons and electrons with $\rho_p^{\rm id} = \rho_e^{\rm id}$ because of charge neutrality. In ionization equation (1), β is the inverse temperature, while m_p and m_e are the proton and electron masses, and $m = m_p m_e/(m_p + m_e)$ is the mass of the reduced particle. All ideal densities can be computed in terms of the sole total electron or proton density $\rho = \rho_e^{\rm id} + \rho_{\rm at}^{\rm id} = \rho_{\rm p}^{\rm id} + \rho_{\rm at}^{\rm id}$ and of the temperature-dependent density

$$\rho^* = \frac{\exp(\beta E_{\rm H})}{2\left(2\pi\lambda_{\rm pe}^2\right)^{3/2}} \quad \text{with} \quad \lambda_{pe} = (\beta\hbar^2/m)^{1/2}, \tag{2}$$

which naturally emerges in ionization equation (1). The resulting Saha equation of state (EOS) follows from adding the partial pressures of the three ideal gases in the mixture, and it reads

$$\beta P_{\rm Saha} = \rho + \rho^*[\sqrt{1 + 2\rho/\rho^*} - 1]\,. \tag{3}$$

Temperature-dependent density ρ^* controls the crossover between full ionization and full recombination, as illustrated by the respective behaviors $\beta P_{\rm Saha} \sim 2\rho$ for $\rho \ll \rho^*$ and $\beta P_{\rm Saha} \sim \rho$ for $\rho \gg \rho^*$. As recalled in Sec. II, within the physical picture, the Saha predictions have been proved to be asymptotically valid in a suitable scaling limit in the grand-canonical ensemble [33], where temperature T is decreased while chemical potentials μ_p and μ_e go to $E_{\rm H}$ with a linear dependence in T. The corresponding density decreases exponentially fast with T, in order to keep the same energy-entropy balance and, hence, the same ionization degree. The identification of that scaling limit opened up the possibility to construct systematic expansions beyond Saha theory [6]. The structure of the corresponding SLT expansion of the density in terms of the chemical potential is described in Sec. II. The successive terms depend on temperature-dependent functions $h_k(\beta)$ which decay exponentially fast when $T \to 0$ with increasing decay rates. Their physical content is discussed in relation with the formation of chemical species, interaction, and screening effects.

In Sec. III, starting from the SLT expansion of density and using standard thermodynamical identities, we derive the SLT expansions of chemical potential, pressure, and internal energy. By construction, all expressions are thermodynamically consistent, and similar expressions for other thermodynamical quantities can be easily derived along similar lines. In those SLT expansions, beyond the leading terms given by Saha theory, each correction reduces to an algebraic function of ratio ρ/ρ^* times a temperature-dependent function which decays exponentially fast when $T \to 0$. We give the expressions of all corrections up to order $\exp(\beta E_{\rm H})$ included. Such corrections account for various phenomena such as plasma polarization, thermal atomic excitations, shift of the atomic energy levels, formation of hydrogen molecules H_2 and ions H^- and H_2^+, and interactions between ionized charges and atoms.

As usual for asymptotic expansions, and aside from the question of convergence in a strict mathematical sense, the truncation of SLT expansions can be reasonably expected to provide reliable quantitative informations on thermodynamics. Here, since the characteristic energy scale $|E_{\rm H}|$ involved in SLT expansions is rather large, the corresponding calculations should be reliable up to temperatures of the order 10^4 K for which the condition $kT \ll |E_{\rm H}|$ is indeed fulfilled. Furthermore, we stress that, though the SLT expansion is built by considering a low-density and low-temperature scaling, it can provide actually accurate predictions in a rather large range of densities and temperatures that cover the fully ionized, partially ionized, and atomic phases of the hydrogen gas. Indeed, the SLT expansion reduces by construction to the standard virial expansion when $\rho \ll \rho^*$ at fixed T [6]. Thus, the SLT formulas remain valid in the fully ionized regime where one may have $T > T_{\rm Rydberg} = |E_{\rm H}|/k = 157\,801$ K, as long as the density is not too high, namely the coupling parameter $\Gamma = \beta e^2/a$ must remain small.

If we keep all corrections to Saha leading terms up to order $\exp(\beta E_{\rm H})$ included, as provided by the SLT formulas, the knowledge of the first four functions $h_1(\beta)$, $h_2(\beta)$, $h_3(\beta)$, and $h_4(\beta)$ is required. If functions $h_1(\beta)$ and $h_3(\beta)$ are explicitly known in closed elementary forms and can be calculated exactly at any temperature, no similar formulas for functions $h_2(\beta)$ and $h_4(\beta)$ are available since analytical results on the three- and four-body quantum problem are very scarce. In Sec. IV, we propose simple approximations of

those functions which account for their exact low-temperature forms, on the one hand, and incorporate the usual reliable descriptions of the spectra of ions H^-, H_2^+ and of molecule H_2, on the other hand. Those approximations are sufficient for computing thermodynamical properties of a partially ionized hydrogen gas for temperatures up to about 30 000 K. More refined calculations of functions $h_2(\beta)$ and $h_4(\beta)$ would be required at higher temperatures, in particular for state points where recombination into hydrogen molecules or ions give a significant contribution.

In Sec. V, within previous simple representations of the $h_k(\beta)$'s, we study the importance of the various nonideal corrections to Saha pressure and internal energy along various isotherms and isochores. The predictions of our analytical SLT formulas are compared to the OPAL tables which, up to now, are expected to provide the most reliable numerical data in the considered regimes. A very good agreement is found at low densities, for all temperatures, if one corrects the OPAL tables by using the exact ground-state energy of the hydrogen atom with the reduced mass m in place of m_e [34]. When the density is increased, our predictions differ somewhat from those of the OPAL tables. We compare also our predictions to data of quantum Monte Carlo simulations [4]. These comparisons, together with a simple semiempirical criterion, allow us to determine the validity domain of the SLT expansion in the temperature-density plane (see Fig. 12). Final comments and possible extensions are given in Sec. VI.

II. THE SCALED LOW-TEMPERATURE EXPANSION

A. The Saha regime in the grand-canonical ensemble

Within the physical picture, a hydrogen gas is viewed as a system of quantum point particles which are either protons or electrons, interacting via the instantaneous Coulomb potential $v(r) = 1/r$. Protons and electrons have respective charges, masses, and spins, $e_p = e$ and $e_e = -e$, m_p and m_e, $\sigma_p = \sigma_e = 1/2$. In the present nonrelativistic limit, the corresponding Hamiltonian for $N = N_p + N_e$ particles reads

$$H_{N_p,N_e} = -\sum_{i=1}^{N} \frac{\hbar^2}{2m_{\alpha_i}} \Delta_i + \frac{1}{2} \sum_{i \neq j} e_{\alpha_i} e_{\alpha_j} v(|\mathbf{x}_i - \mathbf{x}_j|), \quad (4)$$

where $\alpha_i = p,e$ is the species of the ith particle and Δ_i is the Laplacian with respect to its position $\mathbf{x}_i$. The system is enclosed in a box with volume Λ, in contact with a thermostat at temperature T and a reservoir of particles that fixes the chemical potentials equal to μ_p and μ_e for protons and electrons, respectively. Because the infinite system maintains local neutrality $\rho_p = \rho_e$ in any fluid phase, the bulk equilibrium quantities depend in fact solely on the mean,

$$\mu = (\mu_p + \mu_e)/2, \quad (5)$$

while the difference $\nu = (\mu_e - \mu_p)/2$ is not relevant, as rigorously proved in Ref. [35]. Consequently, the common particle density $\rho = \rho_p = \rho_e$ depends only on T and μ.

In the present framework, the EOS (3) has been proved to become exact in some limit introduced by Macris and Martin, who extended Fefferman's work on the atomic phase of the hydrogen plasma [36] to a partially ionized phase [33]. In that limit, the temperature T goes to zero while the average chemical potential μ of protons and electrons approaches the value E_H with a definite slope [33]. More precisely, let γ be the dimensionless parameter defined through the parametrization

$$\mu = E_H + kT\{\ln(\gamma) + \ln[(m/M)^{3/4}/4]\} \quad (6)$$

with $M = m_p + m_e$. The state of the system then is equivalently defined by either the usual set (T,μ) of thermodynamical parameters in the grand-canonical ensemble or the set (T,γ), since both sets are univocally related. As proved in Ref. [33], in the limit $T \to 0$ at fixed γ, density ρ and pressure P behave as ($c > 0$)

$$\rho = \left(\rho_p^{\mathrm{id}} + \rho_{\mathrm{at}}^{\mathrm{id}}\right)[1 + O(e^{-c\beta})] = \left(\rho_e^{\mathrm{id}} + \rho_{\mathrm{at}}^{\mathrm{id}}\right)[1 + O(e^{-c\beta})] \quad (7)$$

and

$$\beta P = \left(\rho_p^{\mathrm{id}} + \rho_e^{\mathrm{id}} + \rho_{\mathrm{at}}^{\mathrm{id}}\right)[1 + O(e^{-c\beta})], \quad (8)$$

where ideal densities reduce to

$$\rho_p^{\mathrm{id}} = \rho_e^{\mathrm{id}} = \rho^* \gamma \quad (9)$$

and

$$\rho_{\mathrm{at}}^{\mathrm{id}} = \rho^* \frac{\gamma^2}{2}. \quad (10)$$

Notice that ideal densities (9) and (10) do satisfy the Saha ionization equation (1) for the total proton/electron density $\rho = \rho^* \gamma(1 + \gamma/2)$. Moreover, the leading contribution to pressure in formula (8) indeed describes an ideal mixture of free protons, free electrons, and hydrogen atoms in their ground state, which can be rewritten in the form Eq. (3). Thus, discarding exponentially vanishing terms embedded in $O(e^{-c\beta})$, Saha predictions are rigorously recovered in the scaling limit of Macris and Martin $T \to 0$ at fixed γ. The parameter γ may be fixed at an arbitrary positive value; it controls the density and also the ionization ratio since $\rho_p^{\mathrm{id}}/\rho = 1/(1 + \gamma/2)$. Contrary to the zero-temperature limit at fixed chemical potential used in the atomic and molecular limit theorem [15,36,37] (see also Ref. [38] for further physical considerations around that limit), we consider γ fixed and a chemical potential that varies as $T \to 0$ according to Eq. (6) so the e-p plasma tends in the limit $T \to 0$ to a partially ionized hydrogen gas with a well-defined ionization ratio.

The Saha regime corresponds to quite diluted conditions, since the densities of ionized particles and of atoms vanish exponentially fast when $\beta \to \infty$, with a rate determined by the ground-state energy of the hydrogen atom $E_H \simeq -13.6$ eV. The low-temperature condition, namely $kT \ll |E_H|$, ensures that atoms can form, while they maintain their individuality thanks to $a \gg a_B$, where $a = (3/(4\pi\rho))^{1/3}$ is the mean interparticle distance and $a_B = \hbar^2/(2me^2)$ is the Bohr radius. Because of the high dilution, the system is both weakly coupled and weakly degenerate. In particular, the ionized charges are almost classical, and the corresponding screening length reduces to its Debye expression $\kappa^{-1} = [4\pi\beta e^2(\rho_p^{\mathrm{id}} + \rho_e^{\mathrm{id}})]^{-1/2}$.

According to the above rigorous derivation, corrections to Saha theory decay exponentially fast in the scaled limit $T \to 0$ at fixed γ. Nevertheless, they cannot be explicitly computed within the corresponding mathematical techniques, so one has to use different tools as described further.

B. About the interplay between recombination and screening

In the Saha regime, in addition to atoms, recombination processes lead to the formation of molecules H_2, ions H^- and $H_2{}^+$, and also more complex entities like $H_2{}^-$, $H_3{}^+$, H_3, and so on. A controlled analysis of the corresponding contributions is the central problem for deriving systematic corrections to Saha theory. The well-known difficulty lies in a suitable account of the individual contribution of a single chemical species at finite temperature, which is free from the divergences arising from Rydberg states. In the literature, in general, that problem has been tackled within phenomenological prescriptions, in particular those leading to the so-called Brillouin-Planck-Larkin formula for atomic contributions [39,40]. The physical idea underlying that phenomenological approach is that the divergent contributions of Rydberg states are in fact screened by the free charges present in the system. Accordingly, the estimation of contributions from recombined entities cannot be disentangled from that of screened interactions between ionized charges.

A systematic procedure for dealing simultaneously with recombination and screening has been constructed through the combination of path integral and diagrammatical methods [21]. This provided some kind of cluster representation for equilibrium quantities in the grand-canonical ensemble. In the quite diluted Saha regime, the statistical weight of a given cluster made with N_p protons and N_e electrons involves the cluster partition function

$$Z(N_p,N_e) = 2\pi\lambda_{N_p,N_e}^2 \lim_{\Lambda\to\infty} \frac{1}{\Lambda} \mathrm{Tr}[\exp(-\beta H_{N_p,N_e})]_{\mathrm{Mayer}}^{T}, \tag{11}$$

which is a truncated trace of Gibbs operator $\exp(-\beta H_{N_p,N_e})$ built with bare Coulomb Hamiltonians, while $\lambda_{N_p,N_e} = (\beta\hbar^2/[N_p m_p + N_e m_e])^{1/2}$ is the thermal de Broglie wavelength of the cluster. The trace in Eq. (11) converges despite the long range of the Coulomb interaction, thanks to a systematic truncation procedure which accounts for the screening by ionized charges [21]. Roughly speaking, that procedure amounts to subtract and add counterterms to the genuine Gibbs operators, which involve nontraceable operators built with the Coulomb potential. The Gibbs operator and the subtracted counterterms give rise to the finite partition function (11) which depends only on T and no longer on γ. The added counterterms are recombined together with other divergent contributions *via* chain resummations, which ultimately provide finite contributions involving the screening length κ^{-1} associated with the ionized charges present in the medium.

Remarkably, the familiar chemical species naturally emerge from cluster partition function $Z(N_p,N_e)$, which is intrinsic to the considered cluster in the vacuum. A given chemical species made with N_p protons and N_e electrons is associated with bound states of bare Hamiltonian H_{N_p,N_e}. In the zero-temperature limit, it provides the leading contribution to $Z(N_p,N_e)$ which behaves as

$$\exp\left(-\beta E_{N_p,N_e}^{(0)}\right) \tag{12}$$

apart from possible integer degeneracy factors and where $E_{N_p,N_e}^{(0)}$ is the groundstate energy of Hamiltonian H_{N_p,N_e}. At finite temperatures, $Z(N_p,N_e)$ involves not only contributions from thermally excited bound states but also contributions from diffusive states describing the dissociation of the considered chemical species.

Cluster partition functions $Z(N_p,N_e)$ can be viewed as generalizations of Ebeling virial coefficients [9] introduced for dealing with contributions from two-particle clusters. The contributions of interactions between chemical species can be expressed also in terms of cluster functions similar to $Z(N_p,N_e)$, so all contributions related to the formation of complex entities are properly taken into account. We stress that, as far as thermodynamical properties are concerned, only the full contribution of $Z(N_p,N_e)$ and of its related screened counterterms makes an unambiguous sense. The considered formalism [21] avoids both arbitrary and uncontrolled definitions of internal partition functions for chemical species, which are key ingredients in phenomenological chemical approaches.[1]

C. Systematic corrections to Saha theory

Within the combination of path integral and diagrammatical methods evoked above [21], systematic corrections to Saha theory have been explicitly computed in Ref. [6]. A pedagogical summary of both rather long papers is given in Ref. [41]. Here, leaving aside the tedious technical details involved in the derivation, we can guess and explain the mathematical structure of the corresponding expansion through simple arguments based on the considerations exposed just earlier.

In the so-called screened cluster representation of particle density ρ [21], any contribution reduces to a graph made with particle clusters connected by screened bonds. The statistical weight of a cluster made with N_p protons and N_e electrons, reduces to, roughly speaking, the product $\exp[\beta(N_p+N_e)\mu]$ of the particle fugacity factors times the cluster partition function $Z(N_p,N_e)$ and times some dressing factor which accounts for collective polarization effects. The integration over the relative distances between particle clusters generate powers of the Debye screening wave number κ, while dressing factors can be also expanded in powers of κ. Since $\exp(\beta\mu)$ is proportional to both γ and $\exp(-\beta|E_{\mathrm{H}}|)$, while κ is proportional to both $\gamma^{1/2}$ and $\exp(-\beta|E_{\mathrm{H}}|/2)$, any contribution reduces to some integer or half-integer power of γ times a temperature-dependent function. The low-temperature behavior of that function results from the competition between factors varying exponentially fast, namely positive powers of $\exp(-\beta|E_{\mathrm{H}}|)$ arising from fugacity factors, positive or negative powers of $\exp(-\beta|E_{\mathrm{H}}|/2)$ arising from screened interactions and polarization effects, and exploding Boltzmann factors $\exp(-\beta E_{N_p,N_e}^{(0)})$ arising from the contribution of bound entities with ground-state energy

[1] Of course, one might express the trace defining $Z(N_p,N_e)$ over the complete basis made with the eigenstates of H_{N_p,N_e}. This would provide a convergent infinite sum of bound-state contributions, which might be identified as an internal partition function. Nevertheless, extending the analysis carried out in Ref. [42], one can rewrite $Z(N_p,N_e)$ as a finite contribution plus another truncated partition function, which would ultimately provide a different internal part. For instance, various atomic partition functions can be extracted from Ebeling virial coefficient [42], including the famous Planck-Larkin-Brillouin expression.

$E^{(0)}_{N_p,N_e} < 0$ in cluster partition functions. In the Saha regime, namely $T \to 0$ with γ fixed, the order of a given contribution is determined by subtle inequalities involving $E^{(0)}_{N_p,N_e}$ and $E_{\rm H}$. The leading contributions to density ρ are easily identified as arising from graphs made with single clusters carrying either one particle (one proton or one electron) or two particles (one proton and one electron), and they are of order $\exp(-\beta|E_{\rm H}|)$. All the other contributions decay exponentially faster, in agreement with the rigorous estimation of order $O(e^{-c\beta})$ for the full deviation to Saha theory. Accordingly, the corresponding SLT expansion for the dimensionless density ρ/ρ^* takes the following mathematical form Ref. [6]:

$$\rho/\rho^* = \gamma + \frac{\gamma^2}{2} + \sum_{k=1}^{\infty} \gamma^{n_k} h_k(\beta). \tag{13}$$

In Eq. (13), the leading first two terms are the ideal contributions predicted by Saha theory, while the sum accounts for the corrections. In each correction with order k, power n_k is integer or half-integer while γ^{n_k} may be multiplied by logarithmic terms. Furthermore, function $h_k(\beta)$ decays exponentially fast in the zero-temperature limit, $h_k(\beta) \sim \exp(-\beta\delta_k)$ when $\beta \to \infty$, except for possible multiplicative powers of β. We stress that expansion (13) is not ordered with respect to powers of γ, i.e., the n_k's do not necessarily increase with k, but it is ordered with respect to increasing decay rates, $0 < \delta_1 < \delta_2 < \ldots$, of functions $h_k(\beta)$. In other words, instead of γ, which is kept fixed here, the small parameter is built with the temperature which is sent to zero. That small parameter may be identified with $\exp(-\beta|E_{\rm H}|)$, so the leading low-temperature behavior of each correction of order k reduces to some positive real power $\delta_k/|E_{\rm H}|$ of that parameter. Notice that each function $h_k(\beta)$ does not reduce to its leading low-temperature form in general, but it also involves contributions which decay exponentially faster than $\exp(-\beta\delta_k)$.

The SLT expansion (13) provides an exact relationship between the density and the chemical potential [recall definition (6) of γ] that is very useful in the Saha regime because the series converges then rapidly and can be safely truncated. We comment on the mathematical form and the physical content of the first four corrections $h_k(\beta)$ in the next subsection. It will then be shown in Sec. III how Eq. (13) can be used to compute explicitly in the Saha regime any thermodynamical quantity as a function of the natural physical variables ρ and T.

D. First corrections and their physical content

The first four functions $h_k(\beta)$ as well as the corresponding n_k's, $k = 1,2,3,4$, are explicitly computed in Ref. [6], where it is also shown that all other h_k's with $k \geqslant 5$ decay faster than $\exp(\beta E_{\rm H})$, i.e., $\delta_k > |E_{\rm H}|$ for $k \geqslant 5$. Thus, if we truncate expansion (13) up to order $\exp(\beta E_{\rm H})$ included, it is consistent to only retain contributions which are at most of that order in the first four h_k's. In the following, we recall the corresponding expressions and we discuss their physical content.

1. *Term $k = 1$: plasma polarization around ionized charges*

That correction arises from a single cluster with one proton (electron) where dressing many-body effects on its statistical weight are computed at leading order. This provides the fugacity factor $\exp(\beta\mu)$ multiplied by the Debye screening factor κ. Accordingly, we find $n_1 = 1 + 1/2 = 3/2$ and $\delta_1 = -(E_{\rm H} + E_{\rm H}/2 - E_{\rm H}) = |E_{\rm H}|/2$, once ρ has been expressed in units of temperature-dependent density $\rho^* \sim \exp(-\beta|E_{\rm H}|)$. The precise form of function $h_1(\beta)$ reads

$$h_1(\beta) = \frac{(\beta|E_{\rm H}|)^{3/4}}{\pi^{1/4}} \exp(\beta E_{\rm H}/2), \tag{14}$$

since $Z(1,0) = Z(0,1) = 2$ for a single proton or a single electron, for which no truncation occurs, namely $[\exp(-\beta H_{1,0})]^T_{\rm Mayer} = \exp(-\beta H_{1,0})$ and $[\exp(-\beta H_{0,1})]^T_{\rm Mayer} = \exp(-\beta H_{0,1})$.

The present correction accounts for the familiar polarization of the plasma surrounding an ionized charge. In the literature, that mechanism was taken into account for the first time in Ref. [43] through a suitable modification of Saha ionization equilibrium (1). We have checked that the corresponding correction to Saha theory can be exactly recovered by keeping only the first term $k = 1$ in the SLT expansion (13).

2. *Term $k = 2$: formation of molecules and atom-atom interactions*

That correction arises from a single cluster made with two protons and two electrons and from two interacting neutral clusters where each of them is made with one proton and one electron. At leading order, dressing collective effects in statistical weights can be neglected, while screening of interactions between neutral clusters can be also omitted since the corresponding bare interactions are integrable. Then, power n_2 is merely determined by the product of four fugacity factors $\exp(\beta\mu)$, which provides $n_2 = 4$. Function $h_2(\beta)$ reduces to

$$h_2(\beta) = \frac{1}{64}\left(\frac{2m}{M}\right)^{3/2} Z(2,2)\exp(3\beta E_{\rm H}) + W(1,1|1,1)\exp(3\beta E_{\rm H}), \tag{15}$$

where $W(1,1|1,1)$ is a suitable trace analogous to expression (11) which now involves two Gibbs operators $\exp(-\beta H_{1,1})$ associated with two proton-electron pairs, as well as their bare Coulomb interactions. Factors $\exp(3\beta E_{\rm H})$ arise from the product of the four fugacity factors $\exp(\beta\mu)$ and the rewriting of ρ in units of ρ^*. In the zero-temperature limit, the leading contribution in expression (15) is that of the molecular ground state in $Z(2,2)$ with energy $E_{\rm H_2} = E^{(0)}_{2,2}$. Notice that, because of inequality $3E_{\rm H} < E_{\rm H_2} < 2E_{\rm H}$, function $h_2(\beta)$ indeed decays exponentially fast with the rate $\delta_2 = |3E_{\rm H} - E_{\rm H_2}| \simeq 9.1$ eV. That inequality ensures that molecules H_2 are very scarce in the Saha regime compared to atoms H, despite that they are more stable energetically, Moreover, δ_2 is indeed larger than $\delta_1 = |E_{\rm H}|/2 \simeq 6.8$ eV.

Molecular contributions are embedded in $Z(2,2)$, which is indeed finite thanks to the truncation procedure inherited from screening, as well as the short-range part of atom-atom interactions. Long-range atom-atom interactions, including familiar van der Waals interactions, appear in $W(1,1|1,1)$. Notice that the screened counterterms related to the truncations involved here provide contributions to expansion (13) which decay faster than $\exp(\beta E_{\rm H})$, and they arise in terms with

$k \geqslant 5$. We stress that both molecular formation and atom-atom interactions are properly taken into account, without any *a priori* modelizations like in usual chemical approaches. Here the corresponding contributions are expressed in terms of the associated few-body Coulomb Hamiltonians, and they naturally emerge through the fundamental quantum mechanisms at work. In particular, the quantum mechanical operators involved in both $Z(2,2)$ and $W(1,1|1,1)$ automatically and correctly take care of the unavoidable mixing between the contributions from two interacting atoms, on the one hand, and from a single molecule, on the other hand.

3. *Term k = 3: atomic excitations and charge-charge interactions*

That correction arises from single clusters made with either one or two particles. Contributions of two-particle clusters are controlled by the product of two fugacity factors $\exp(\beta\mu)$ and of two-body cluster partition functions $Z(2,0)$, $Z(0,2)$, and $Z(1,1)$, while contributions from the one-particle clusters reduce to one fugacity factor $\exp(\beta\mu)$ multiplied by a factor κ^2 which accounts for polarization effects beyond the Debye mean-field result of order κ. This leads to $n_3 = 1 + 1 = 1 + 2 \times 1/2 = 2$ and

$$h_3(\beta) = -\frac{1}{2} + \left[1 + \frac{1}{12}\ln\left(\frac{4m}{M}\right)\right]\frac{(\beta|E_{\rm H}|)^{3/2}}{\pi^{1/2}}\exp(\beta E_{\rm H}) + \frac{1}{8\pi^{1/2}}\left\{2Q(x_{pe}) + \left(\frac{2m}{m_p}\right)^{3/2} \times \left[Q(-x_{pp}) - \frac{1}{2}E(-x_{pp})\right] + \left(\frac{2m}{m_e}\right)^{3/2}[Q(-x_{ee})] - \frac{1}{2}E(-x_{ee})]\right\}\exp(\beta E_{\rm H}), \quad (16)$$

where the two-particle partition functions, $Z(2,0)$, $Z(0,2)$ and $Z(1,1)$ have been rewritten in terms of Ebeling's functions $Q(x)$ and $E(x)$ [9] with $x_{pe} = 2(\beta|E_{\rm H}|)^{1/2}$, $x_{pp} = (2m_p/m)^{1/2}(\beta|E_{\rm H}|)^{1/2}$, and $x_{ee} = (2m_e/m)^{1/2}(\beta|E_{\rm H}|)^{1/2}$. The ground-state contribution has been extracted from $Z(1,1)$ and it provides the leading atomic contribution $\gamma^2/2$ in Eq. (13). Consequently, the leading low-temperature behavior of $h_3(\beta)$ arises from the contribution to $Q(x_{pe})$ of the first excited state of an atom H with energy $E_{\rm H}/4$, so δ_3 reduces to $\delta_3 = -E_{\rm H}/4 + E_{\rm H} = -3E_{\rm H}/4$. That decay rate $\delta_3 \simeq 10.2$ eV is indeed larger than $\delta_2 \simeq 9.1$ eV.

The present correction involves contributions of the atomic excited states, as well as of interactions between two ionized charges. The screened long-range part of such interactions are precisely the counterterms related to the truncations ensuring the finiteness of $Z(2,0)$, $Z(0,2)$, and $Z(1,1)$ or, equivalently, of the Ebeling function Q.

4. *Term k = 4: formation of ions and atom-charge interactions*

That correction arises from single three-particle clusters, a two-particle cluster interacting with a one-particle cluster, and a single two-particle cluster dressed by many-body effects. All contributions provide the same power $n_4 = 3$ of γ, as resulting from either the product of three fugacity factors $\exp(\beta\mu)$ or the product of two fugacity factors $\exp(\beta\mu)$ times a factor κ^2 arising from polarization effects, namely $n_4 = 1 + 1 + 1 = 1 + 1 + 2 \times 1/2 = 3$. The corresponding function $h_4(\beta)$ reads

$$h_4(\beta) = \frac{3}{64}\left\{\left[\frac{m_e(M+m_p)}{M^2}\right]^{3/2} Z(2,1) + \left[\frac{m_p(M+m_e)}{M^2}\right]^{3/2} \times Z(1,2)\right\}\exp(2\beta E_{\rm H}) + S_3(1,1)\exp(2\beta E_{\rm H}) + \frac{3}{2}[W(1,1|1,0) + W(1,1|0,1)]\exp(2\beta E_{\rm H}). \quad (17)$$

The leading low-temperature behavior of $h_4(\beta)$ arises from the ground-state contribution of ion $H_2{}^+$ in $Z(2,1)$, so $\delta_4 = E_{H_2{}^+} - 2E_{\rm H} \simeq 11.0$ eV, which is indeed larger than $\delta_3 \simeq 10.2$ eV.

Several phenomena contribute to the present correction. First, formation of ions $H_2{}^+$ and H^- are embedded in partition functions $Z(2,1)$ and $Z(1,2)$, respectively. Second, contributions of bare interactions between an atom H and a single ionized charge are described by the functions $W(1,1|1,0)$ and $W(1,1|0,1)$. Third, the function $S_3(1,1)$ accounts for modifications of the atomic ground state due to the polarization of the surrounding plasma, beyond the familiar Debye shift.

III. THERMODYNAMICAL FUNCTIONS

A. Chemical potential as a function of density

In physical systems, the natural thermodynamical parameters are the temperature and the density. Thus, it is quite useful to invert the SLT expansion (13), namely to determine $\gamma(\rho,T)$. Then, by using standard thermodynamical identities, we are able to compute consistently all thermodynamical quantities as functions of T and ρ. In the present low-temperature limit, the inversion can be performed in a perturbative way as follows. First, if we neglect all the exponentially small corrections embedded in the h_k's, the density reduces to its Saha expression,

$$\rho/\rho^* = \gamma + \frac{\gamma^2}{2}. \quad (18)$$

The inversion of that relation, which amounts here to solving a simple second-order equation for γ, gives

$$\gamma_{\rm Saha}(\rho,T) = \gamma_{\rm S}(\xi) = \sqrt{1+2\xi} - 1 \ \text{ with } \ \xi = \rho/\rho^*, \quad (19)$$

which is the leading form of $\gamma(\rho,T)$ in the Saha regime. The inversion of the full relation (13) is then achieved by writing $\gamma(\rho,T) = \gamma_{\rm Saha}(\rho,T)$ plus a small correction which is treated perturbatively. This leads to

$$\gamma(\rho,T) = \sqrt{1+2\rho/\rho^*} - 1 + \sum_{k=1}^{\infty} a_k(\rho/\rho^*)g_k(\beta), \quad (20)$$

where a_k depends only on $\xi = \rho/\rho^*$, while g_k depends only on temperature. The a_k's can be determined in terms of $\gamma_{\rm S}(\xi)$ and of its derivatives with respect to ξ. Each g_k reduces to a polynomial in the h_l's with $1 \leqslant l \leqslant k$. Thus, the g_k's decay exponentially fast when $\beta \to \infty$, and they are ordered with respect to increasing decay rates. The first five terms in Eq. (20) are

$$a_1 = -\frac{\gamma_S^{3/2}}{1+\gamma_S}; \quad a_2 = -\frac{\gamma_S^4}{1+\gamma_S}; \quad a_3 = -\frac{\gamma_S^2}{1+\gamma_S}; \quad a_4 = -\frac{\gamma_S^3}{1+\gamma_S}; \quad a_5 = \frac{\gamma_S^2(2\gamma_S+3)}{2(1+\gamma_S)^3} \tag{21}$$

$$g_1 = h_1; \quad g_2 = h_2; \quad g_3 = h_3; \quad g_4 = h_4; \quad g_5 = h_1^2, \tag{22}$$

where γ_S is given by the simple algebraic function (19) of ρ/ρ^*. All g_k's with $k \geqslant 6$ decay exponentially faster than $\exp(\beta E_H)$.

Similarly to SLT expansion (13), the small parameter in series (20) is the temperature or, equivalently, the exponentially small factor $\exp(-\beta|E_H|)$. Now, the fixed parameter is the ratio $\xi = \rho/\rho^*$ which can take arbitrary values. The corresponding expansion of chemical potential μ straightforwardly follows by inserting series (20) into relation (6). Other thermodynamical functions can be expanded in a similar way by using thermodynamical identities, as explained further for pressure and internal energy.

B. Pressure

We start from the standard relation in the grand-canonical ensemble which expresses the density as the derivative of the pressure with respect to the fugacity $z = \exp(\beta\mu)$. According to the variable change defined through relation (6), that identity can be rewritten as

$$\rho = \frac{\gamma}{2}\frac{\partial \beta P}{\partial \gamma}, \tag{23}$$

where the partial derivative is taken at fixed β. Replacing ρ by its SLT expansion (13) into the right-hand side of identity (23), we easily obtain

$$\beta P/\rho^* = 2\gamma + \frac{\gamma^2}{2} + \sum_{k=1}^{\infty} \frac{2\gamma^{n_k}}{n_k} h_k(\beta), \tag{24}$$

where we have that ρ^* depends only on β, while $\beta P/\rho^*$ vanishes for infinite dilution, namely for $\gamma = 0$. Replacing each factor γ by the SLT inverted series (20), we recast expression (24) as the SLT expansion of the pressure at fixed ratio ρ/ρ^*, namely

$$\beta P/\rho^* = \beta P_{\text{Saha}}/\rho^* + \sum_{k=1}^{\infty} \beta P_k/\rho^*. \tag{25}$$

The leading term is nothing but the well-known Saha pressure (3) in units of ρ^*. The general structure of the k^{th} correction reads

$$\beta P_k/\rho^* = b_k(\rho/\rho^*)\alpha_k(\beta), \tag{26}$$

where α_k is a polynomial in the $h_l(\beta)$'s with $l \leqslant k$. Therefore, for a fixed ratio ρ/ρ^*, corrections $\beta P_k/\rho^*$ decay exponentially fast when $\beta \to \infty$, while the corresponding decay rates increase with k. The functions $[b_k(\rho/\rho^*), \alpha_k(\beta)]$ involved in the first five corrections read

$$b_1 = \frac{\gamma_S^{3/2}(\gamma_S-2)}{3(1+\gamma_S)}; \quad b_2 = -\frac{\gamma_S^4(\gamma_S+3)}{2(1+\gamma_S)}; \quad b_3 = -\frac{\gamma_S^2}{1+\gamma_S}; \quad b_4 = -\frac{\gamma_S^3(\gamma_S+4)}{3(1+\gamma_S)}; \quad b_5 = \frac{\gamma_S^2(2-\gamma_S^2)}{2(1+\gamma_S)^3} \tag{27}$$

$$\alpha_1 = h_1; \quad \alpha_2 = h_2; \quad \alpha_3 = h_3; \quad \alpha_4 = h_4; \quad \alpha_5 = h_1^2, \tag{28}$$

while next correction $\beta P_6/\rho^*$ decays faster than $\exp(\beta E_H)$.

C. Internal energy

In the grand-canonical ensemble and for a finite volume Λ, we set $\langle N\rangle = (\langle N_p\rangle + \langle N_e\rangle)/2$ for the average common number of protons and electrons. We then define, in the thermodynamic limit, the internal energy per particles pair $u = \lim_{TL} U/\langle N\rangle$. Standard thermodynamical identities provide the relation

$$u = \frac{\partial}{\partial\beta}\left(2\beta\mu - \frac{\beta P}{\rho}\right), \tag{29}$$

where the partial derivative with respect to β is taken at fixed density ρ. Inserting into identity (29) the expression (6) of the chemical potential in terms of γ and β, we find

$$u = \left(2 - \frac{\beta P}{\rho}\right) E_H + \frac{3P}{2\rho} + 2\frac{\partial}{\partial\beta}\ln\gamma - \frac{\rho^*}{\rho}\frac{\partial}{\partial\beta}\frac{\beta P}{\rho^*}, \tag{30}$$

where we have also used

$$\frac{\partial}{\partial\beta}\rho^* = (E_H - 3kT/2)\rho^*, \tag{31}$$

inferred from definition (2) of ρ^*. The insertion of expansions (20) and (25) of γ and $\beta P/\rho^*$ into relation (30) provide the corresponding SLT expansion of u. The partial derivatives with respect to β give rise to functions $h_k'(\beta) = dh_k/d\beta$, which decay exponentially fast at low temperatures with the same decay rates as the $h_k(\beta)$'s. Moreover, since ρ^* depends on β, coefficients $a_k(\rho/\rho^*)$ and $b_k(\rho/\rho^*)$ also provide contributions to the partial derivatives with respect to β at fixed ρ. After straightforward algebraic calculations, we eventually obtain

$$u = u_{\text{Saha}} + \sum_{k=1}^{\infty} u_k \tag{32}$$

with

$$u_{\text{Saha}} = (1+\gamma_S\xi^{-1})3kT/2 + (1-\gamma_S\xi^{-1})E_H, \tag{33}$$

and

$$u_1 = -\gamma_S^{1/2}(1+\gamma_S)^{-1}[(1+\gamma_S\xi^{-1})kT + 2(1-\gamma_S\xi^{-1})E_H] \times h_1(\beta), \tag{34}$$

$$u_2 = -\gamma_S^4\xi^{-1}h_2'(\beta)/2 + \gamma_S^3(1+\gamma_S)^{-1}(1+\gamma_S\xi^{-1}/2) \times \left(E_H - \tfrac{3}{2}kT\right)h_2(\beta), \tag{35}$$

$$u_3 = -\gamma_S^2\xi^{-1}h_3'(\beta) + \gamma_S^2\xi^{-1}(1+\gamma_S)^{-1}\left(E_H - \tfrac{3}{2}kT\right)h_3(\beta),$$

$$u_4 = -2\gamma_S^3\xi^{-1}h_4'(\beta)/3 + 2(1+\gamma_S\xi^{-1})\gamma_S^2(1+\gamma_S)^{-1} \times \left(E_H - \tfrac{3}{2}kT\right)h_4(\beta)/3, \tag{37}$$

$$u_5 = (1+\gamma_S)^{-3}\left(3\xi\, kT + \gamma_S^2(3\gamma_S+4)(2+\gamma_S)^{-1}\, E_H\right) \times [h_1(\beta)]^2. \tag{38}$$

Expression (33) of Saha internal energy can be easily interpreted as follows. Let $x_p^{\text{id}} = \rho_p^{\text{id}}/\rho$, $x_e^{\text{id}} = \rho_e^{\text{id}}/\rho$, and $x_{\text{at}}^{\text{id}} = \rho_{\text{at}}^{\text{id}}/\rho$ be the respective molar fractions of ionized protons,

ionized electrons, and hydrogen atoms. We can rewrite formula (33) as

$$u_{\rm Saha} = \left(x_p^{\rm id} + x_e^{\rm id}\right)3kT/2 + x_{\rm at}^{\rm id}(E_{\rm H} + 3kT/2), \quad (39)$$

so each ionized charge does provide a classical kinetic contribution $3kT/2$, while each atom does provide the kinetic contribution $3kT/2$ associated with motion of its mass center plus the ground-state energy $E_{\rm H}$, as it should. Notice that the low-temperature behavior of corrections (35) and (37) can be similarly interpreted in terms of the contributions of molecules H_2 and ions H^-, $H_2{}^+$ respectively.

Other equilibrium quantities can also be derived from previous expansions *via* thermodynamical identities, like the specific heats, or the isentropic compressibility which determines the sound speed. Such derivations are, of course, consistent within the general framework of thermodynamics: A given quantity can be computed following different routes which all lead to the same expression.

IV. REPRESENTATIONS OF TEMPERATURE-DEPENDENT FUNCTIONS

For practical applications of SLT expansions, we need simple representations of functions $h_k(\beta)$ at finite temperatures. Though asymptotic low-temperature behaviors of such functions are exactly known for $k = 1,2,3,4$, explicit analytic expressions at finite temperature are available only for $h_1(\beta)$ and $h_3(\beta)$, thanks to our exact knowledge of the whole spectrum of two-body Coulomb Hamiltonians (see Sec. IV A). For functions $h_2(\beta)$ and $h_4(\beta)$, we construct simple approximations which are expected to be sufficiently accurate for temperatures up to 30 000 K (see Sec. IV B). Eventually, we provide the corresponding numerical tables and plots for all those functions.

A. Analytical expressions for one- and two-body functions

Function $h_1(\beta)$ is given by the simple formula (14) which reduces to an elementary function of dimensionless parameter $\beta E_{\rm H}$. Function $h_3(\beta)$ is given by expression (16) in terms of Ebeling virial functions $Q(x)$ and $E(x)$, which have been widely studied in the literature. In particular, entire series expansions in powers of x have been derived [44,45],

$$Q(x) = -\frac{1}{6}x - \frac{\sqrt{\pi}}{8}x^2 - \frac{1}{6}\left(\frac{C}{2} + \ln 3 - \frac{1}{2}\right)x^3 + \sum_{n=4}^{\infty} q_n x^n,$$
$$q_n = \sqrt{\pi}\frac{\zeta(n-2)}{2^n\Gamma\left(\frac{n}{2}+1\right)}, \quad (40)$$

where $C = 0.57721\ldots$ is the Euler-Mascheroni constant and $\zeta(s)$ is Riemann's function, while

$$E(x) = \frac{1}{2} + \frac{\sqrt{\pi}\ln 2}{4}x^2 + \frac{\pi^2}{72}x^3 + \sum_{n=4}^{\infty} e_n x^n,$$
$$e_n = \sqrt{\pi}(1 - 2^{2-n})\frac{\zeta(n-1)}{2^n\Gamma\left(\frac{n}{2}+1\right)} \quad (41)$$

with x replaced by $x_{pe} = 2(\beta|E_{\rm H}|)^{1/2}$, $-x_{pp} = -(2m_p/m)^{1/2}(\beta|E_{\rm H}|)^{1/2}$, or $-x_{ee} = -(2m_e/m)^{1/2}(\beta|E_{\rm H}|)^{1/2}$. Since x is proportional to $1/\sqrt{T}$, such series can be viewed as high-temperature expansions. A controversy has arisen recently on Eq. (40), with Kraeft [46] and Kremp, Schlanges, and Kraeft [13] maintaining that no linear term $-x/6$ should be present. Starting from the definition of function $Q(x)$ see, for instance, Eq. (7.1) in Ref. [23], one can calculate quite easily its high-temperature behavior by using the Feynman-Kac representation [47] of the density matrix

$$\langle \boldsymbol{r}|e^{-\beta h}|\boldsymbol{r}\rangle = \frac{1}{(2\pi\lambda^2)^{3/2}}\int D(\boldsymbol{\xi})\, e^{\beta e^2\int_0^1 ds\, v(|\boldsymbol{r}+\lambda\boldsymbol{\xi}(s)|)}, \quad (42)$$

where h is the Hamiltonian of a particle of mass m in the attractive Coulomb potential $-e^2/r$ and $\boldsymbol{\xi}(s)$ is a Brownian bridge distributed according to the Wiener measure $D_W(\boldsymbol{\xi})$. At high temperatures, the exponential can be linearized, and a straightforward calculation confirms that the leading behavior is indeed given by Ebeling's result, $-x/6$. Asymptotic large-x, i.e., low-temperature, expansions read

$$Q(x) = 2\sqrt{\pi}\left[\sum_{n=1}^{\infty} n^2\left(e^{x^2/(4n^2)} - 1 - \frac{x^2}{4n^2}\right) - \frac{x^2}{8}\right]$$
$$- \frac{x^3}{6}\left(\ln x + 2C + \ln 3 - \frac{11}{6}\right) - \frac{x}{12}$$
$$- \frac{1}{60x} + O\left(\frac{1}{x^3}\right) \quad (43)$$

for $x > 0$ (attractive case) and

$$Q(x) = -\frac{x^3}{6}\left(\ln|x| + 2C + \ln 3 - \frac{11}{6}\right) - \frac{x}{12}$$
$$- \frac{1}{60x} + O\left(\frac{1}{x^3}\right) \quad (44)$$

for $x < 0$ (repulsive case). When $x \to -\infty$, a semiclassical calculation [48] shows that exchange function $E(x)$ decays exponentially fast as

$$E(x) \simeq \frac{4}{\sqrt{3\pi}}|x|\exp\left[-\frac{3}{2}\left(\pi^2\frac{x^2}{2}\right)^{1/3}\right]. \quad (45)$$

As far as numerical calculations are concerned, high-temperature series (40) and (41) are quite useful because their radius of convergence is infinite. When x becomes very large, calculations using large-x expansions (43)–(45) are, of course, faster. Those low-temperature expansions can be used in fact to compute $h_3(T)$ from formula (16), up to the Rydberg temperature $|E_{\rm H}|/k \simeq 157\,800$ K since $|x_{\rm ab}|$, for ab $= ep, pp, ee$, remains larger than 1. Figure 1 shows a plot of functions $Q(x)$ and $E(x)$.

Notice that the first sum in the right-hand side of expression (43) is nothing but the so-called Brillouin-Planck-Larkin partition function

$$Z_{\rm BPL}(T) = \sum_{n=1}^{\infty} n^2\left(e^{-\beta E_{\rm H}/n^2} - 1 + \frac{\beta E_{\rm H}}{n^2}\right), \quad (46)$$

which was introduced in the 1930s on the basis of heuristic arguments as discussed in Refs. [49,50]. It turns out that $Q(x_{pe}) = Q(T)$ may be approximated by $Z_{\rm BPL}(T)$ if the temperature is not too high [49,51]. Notice that the leading asymptotic behavior of $Q(T)$ and $Z_{\rm BPL}(T)$ are identical as

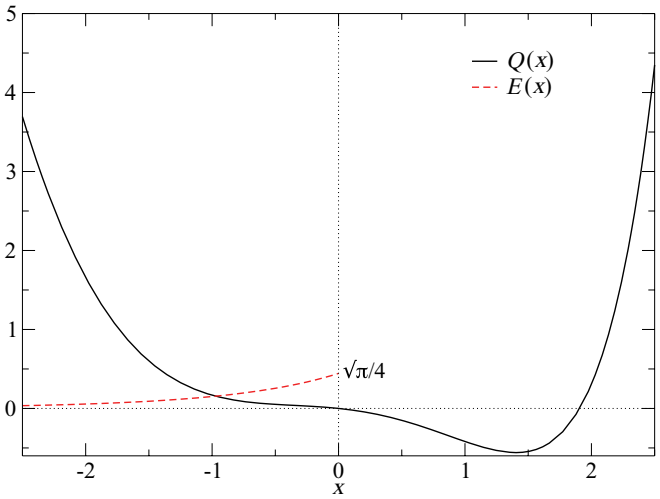

FIG. 1. (Color online) Plot of Ebeling direct and exchange functions $Q(x)$ (solid line) and $E(x)$ (dashed line).

$T \to 0$, whereas one has $Q(T) \sim 1/\sqrt{T}$ versus $Z_{\mathrm{BPL}}(T) \sim 1/T^2$ at high temperatures. The quality of that approximation, and of two even simpler approximations, is shown in Fig. 2. The relative error when approximating $Q(T)$ by $Z_{\mathrm{BPL}}(T)$ is less than 3% for $T \leqslant 25\,000$ K, while it reaches 30% at 50 000 K. Truncating the sum in $Z_{\mathrm{BPL}}(T)$ at $n = 1$ provides actually a better approximation that exhibits an accuracy of 8% at 50 000 K (see Fig. 2). The latter approximation is quite successful because contributions from diffusive states and from terms associated with screening effects in $Q(T)$, more or less cancel out the contributions from excited bound states at the considered temperatures. We stress that our further calculations do not use those approximations but rather the exact expressions for $Q(x)$ recalled earlier.

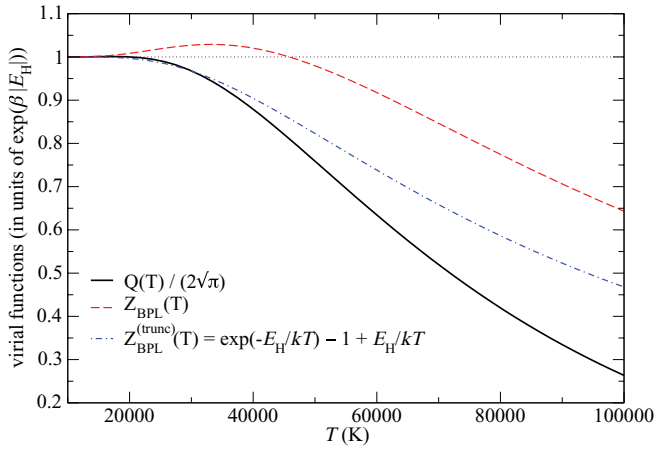

FIG. 2. (Color online) Comparison of the Brillouin-Planck-Larkin partition function (dashed line) to the exact virial function $Q(x_{pe}(T))$ (solid line) for temperatures up to 100 000 K. Truncating the sum in Z_{BPL} after the first term yields a quite good approximation (dot-dashed line). The dotted line (constant value 1) corresponds to keeping only the ground-state contribution $\exp(-E_{\mathrm{H}}/kT)$.

B. Simple approximations for three- and four-body functions

Because of our rather poor knowledge of the whole spectrum of three- and four-body Coulomb Hamiltonians, closed analytical expressions for $h_2(\beta)$ and $h_4(\beta)$ cannot be derived at the moment. So here we proceed to simple estimations of those functions, inspired by the above considerations on $Z(1,1)$, which should work reasonably well in the temperature range considered here.

1. Case of $h_2(\beta)$

The relative importance of the contributions of the various operators involved in $[\exp(-\beta H_{2,2})]^T_{\mathrm{Mayer}}$, the trace of which defines partition function $Z(2,2)$, can be readily estimated by using the ground-state energies of Hamiltonians $H_{2,2}$, $H_{2,1}$, $H_{1,2}$, $H_{1,1}$, $H_{1,0}$, and $H_{0,1}$. Up to 30 000 K, it is sufficient to retain only contributions from $\exp(-\beta H_{2,2})$ and from subtracted operators involving $\exp(-\beta H_{1,1})\exp(-\beta H_{1,1})$. All other combinations of Gibbs operators associated with products of molecular dissociation differing from two atoms, like $\exp(-\beta H_{1,0})\exp(-\beta H_{1,2})$ associated with (p,H^-) or $\exp(-\beta H_{0,1})\exp(-\beta H_{2,1})$ associated with $(e,\mathrm{H_2}^+)$, can be safely neglected. After adding to $Z(2,2)$ the contribution of $W(1,1|1,1)$ in the expression (15) of $h_2(\beta)$, we find that terms which involve imaginary-time evolutions of $V_{\mathrm{at,at}}$, $V^2_{\mathrm{at,at}}$, and $V^3_{\mathrm{at,at}}$ cancel out. This provides a simple estimation of $h_2(\beta)$ as arising entirely from operator $[\exp(-\beta H_{2,2}) - \exp(-\beta H_{1,1})\exp(-\beta H_{1,1})]$.

Similarly to the case of $Z(1,1)$, in the considered temperature range, the main contributions from $[\exp(-\beta H_{2,2}) - \exp(-\beta H_{1,1})\exp(-\beta H_{1,1})]$ can be reasonably expected to arise from the lowest-energy molecular bound states. In addition, we describe such states within the familiar picture where the electrons are in their ground state, while global rotations and vibrations of the molecule are taken into account within a rigid-rotator model and a harmonic oscillator, respectively. This leads to the approximation

$$h_2(\beta) \simeq \frac{\sqrt{2}m^{3/2}}{32M^{3/2}} Z_{\mathrm{H_2}} \exp(3\beta E_{\mathrm{H}}), \tag{47}$$

where the molecular partition function $Z_{\mathrm{H_2}}$ factorizes into [52]

$$Z_{\mathrm{H_2}} = \exp\left(-\beta E_{\mathrm{H_2}}\right) Z^{(\mathrm{rot})}_{\mathrm{H_2}} Z^{(\mathrm{vib})}_{\mathrm{H_2}} \tag{48}$$

with the vibrational part

$$Z^{(\mathrm{vib})}_{\mathrm{H_2}} = \frac{1}{1 - \exp\left(-\beta\epsilon^{(\mathrm{vib})}_{\mathrm{H_2}}\right)} \tag{49}$$

and the rotational part

$$Z^{(\mathrm{rot})}_{\mathrm{H_2}} = \left[\sum_{l=0}^{\infty}(4l+1)\exp\left(-2l(2l+1)\beta\epsilon^{(\mathrm{rot})}_{\mathrm{H_2}}\right) + 3\sum_{l=0}^{\infty}(4l+3)\exp\left(-(2l+1)(2l+2)\beta\epsilon^{(\mathrm{rot})}_{\mathrm{H_2}}\right)\right]. \tag{50}$$

In formula (50), the first sum runs over rotational states of parahydrogen and the second sum over rotational states of orthohydrogen. The energy quanta $\epsilon^{(\mathrm{vib})}_{\mathrm{H_2}} = kT^{(\mathrm{vib})}_{\mathrm{H_2}}$ and $\epsilon^{(\mathrm{rot})}_{\mathrm{H_2}} = kT^{(\mathrm{rot})}_{\mathrm{H_2}}$ associated to proton vibrations and global rotations are

TABLE I. Spectroscopic data of some hydrogen bound states: ground-state energy $E^{(0)}$ (in atomic units) and rotational and vibrational temperatures (in K). The values include neither relativistic nor radiative corrections.

	H	H^-	H_2	H_2^+	H_2^-	H_3^+
$E^{(0)}$	−0.5	−0.527733147	−1.164663172	−0.597139063	−1.048274	-1.323 ± 0.002
$T^{(\mathrm{rot})}$	/	/	85.26	41.87	50.42	(not used[a])
$T^{(\mathrm{vib})}$			5986.98	3150.78	2228.32	
Ref.		[b]	[c]	[d]	[e]	[f]

[a]For the rovibrational partition function of H_3^+, see L. Neale and J. Tennyson, *Astrophys. J.* **454**, L169 (1995).
[b]*Handbook of Atomic, Molecular, and Optical Physics*, edted by G. Drake (Springer, 2006).
[c]L. Wolniewicz, J. Chem. Phys. **99**, 1851 (1993).
[d]J. Ph. Karr and L. Hilico, J. Phys. B: At. Mol. Opt. Phys. **39**, 2095 (2006).
[e]Calculated by V. Robert using a coupled cluster [CCSD(T)] approach including an extended basis set for hydrogen atoms ($4s3p2d1f$).
[f]P. C. Cosby and H. Helm, Chem. Phys. Lett. **152**, 71 (1988).

listed in Table I. We recall that the rotational partition function reduces to the classical result

$$Z_{\mathrm{H_2}}^{(\mathrm{rot})} \sim \frac{2T}{T_{\mathrm{H_2}}^{(\mathrm{rot})}}, \tag{51}$$

when $T \gg T_{\mathrm{H_2}}^{(\mathrm{rot})}$. Notice that more precise descriptions of the lowest-energy excited states of H_2, which do not neglect rotation-vibration coupling as the rigid rotor approximation (48), are available in the literature [53] but are not required for our purpose.

Approximation (47) can be viewed as a suitable extrapolation of the the exact low-temperature behavior of $h_2(\beta)$, which includes both leading and sub-leading terms. Up to 30 000 K, contributions of electronic excitations can be omitted because the corresponding energy gaps are of order 10 eV at least. Moreover, and similarly to the case of $Z(1,1)$, either diffusive states like those associated with the dissociation of the molecule into two atoms or substracted terms involved in the truncated operator $[\exp(-\beta H_{2,2})]^T_{\mathrm{Mayer}}$ like $\exp(-\beta H_{1,1})\exp(-\beta H_{1,1})$ provide contributions which can be safely neglected in that relatively low-temperature range. As detailed in Appendix, this has been checked within a simplified model which is often used for describing the energy levels of the molecule H_2.

2. *Case of $h_4(\beta)$*

Function $h_4(\beta)$, defined by formula (17), can be approximated within a construction similar to the above derivation for $h_2(\beta)$. This provides

$$\begin{aligned} h_4(\beta) \simeq & \frac{3m_e^{3/2}(M+m_p)^{3/2}}{64M^3} Z_{\mathrm{H_2^+}} \exp(2\beta E_{\mathrm{H}}) \\ & + \frac{3m_p^{3/2}(M+m_e)^{3/2}}{64M^3} Z_{\mathrm{H^-}} \exp(2\beta E_{\mathrm{H}}) \\ & + \frac{c_{\mathrm{at}}}{8\pi^{3/2}(\beta|E_{\mathrm{H}}|)^{1/2}} \exp(\beta E_{\mathrm{H}}), \end{aligned} \tag{52}$$

which is the analog of expression (47) for $h_2(\beta)$. Here, internal partition functions for ions H_2^+ and H^-, which arise from $Z(2,1)$ and $Z(1,2)$, read

$$Z_{\mathrm{H_2^+}} = 2\exp(-\beta E_{\mathrm{H_2^+}}) Z_{\mathrm{H_2^+}}^{(\mathrm{rot})} Z_{\mathrm{H_2^+}}^{(\mathrm{vib})} \tag{53}$$

and

$$Z_{\mathrm{H^-}} = 2\exp(-\beta E_{\mathrm{H^-}}), \tag{54}$$

where the required spectroscopic data are given in Table I, while the contribution of $S_3(1,1)\exp(2\beta E_{\mathrm{H}})$ has been replaced by its low-temperature form with constant $c_{\mathrm{at}} \simeq 10.065$ [6].

Similarly to formula (47), approximate expression (52) incorporates both leading and subleading contibutions to the low-temperature representation of $h_4(\beta)$. A similar accuracy for that approximation can be reasonable expected up to a few thousands kelvins, where ionic ground-state contributions dominate. However, when temperature is increased up to 30 000 K, approximation (52) becomes surely less accurate than its counterpart (47) for $h_2(\beta)$. Indeed, the binding energies of ions H_2^+ and H^- are of order 2.6 and 0.7 eV, respectively, so contributions of all terms which arise from diffusive states, truncations defining $Z(2,1)$ and $Z(1,2)$, or interactions involved in $W(1,1|1,0)$ and $W(1,1|0,1)$ can no longer be neglected for $T > 10\,000$ K. Nevertheless, the accuracy of approximation (52) should be sufficient for our purpose, because contributions to thermodynamics associated with $h_4(\beta)$ remain quite small in the considered density-temperature range.

C. Numerical values and plots

Using the exact representations for $h_1(\beta)$ and $h_3(\beta)$, as well as the approximate forms of $h_2(\beta)$ and $h_4(\beta)$, we can compute those functions easily and quickly. The corresponding plots, in logarithmic units, are shown in Fig. 3, while numerical values at some specific temperatures are given in Table II. Functions $h_2(\beta)$ and $h_4(\beta)$ are computed only up to 30 000 K, because their approximate expressions introduced in Sec. IV B are expected to become inaccurate at higher temperatures.

At low temperatures, all functions are positive and increase monotonously with T up to 30 000 K. Function h_3 changes sign near 90 000 K, while a change of sign in functions h_2 and h_4 might also happen at temperatures above 30 000 K. In function h_4, the contributions arising from ions H_2^+ and H^- have the same order of magnitude and are much larger than the third contribution in Eq. (52) which accounts for a shift in the atomic ground state. For $T < 30\,000$ K, all functions remain quite small in relation with their exponential decay in the zero-temperature limit. The hierarchy $h_1(\beta) \gg h_2(\beta) \gg h_3(\beta) \gg$

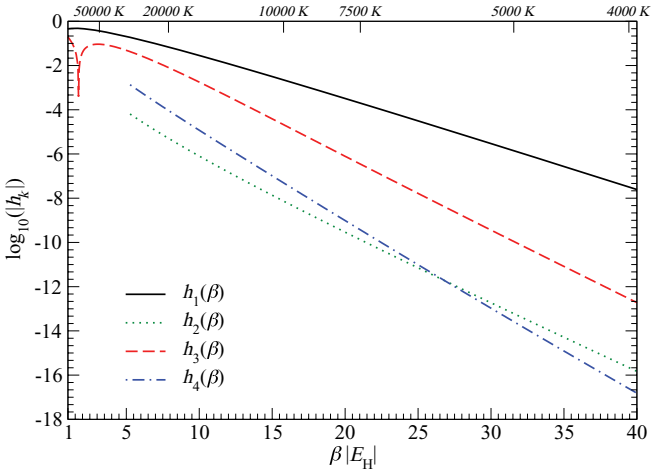

FIG. 3. (Color online) Plot of functions $h_k(\beta)$ for $k = 1,2,3,4$. Note that $\beta|E_H| = T_{\text{Rydberg}}/T$.

$h_4(\beta)$ is satisfied at very low temperature, in agreement with the ordering of the corresponding low-temperature decay rates $\delta_1 < \delta_2 < \delta_3 < \delta_4$. When the temperature is increased, the relative differences between those functions are reduced. In particular, h_3 overcomes h_2 near 1000 K, and h_4 overcomes h_2 near 5900 K.

The ordering of the h_k functions is connected to the relative importance of the corresponding corrections to the ideal Saha equation in the SLT limit $T \to 0$. At finite temperature and density, the ordering of the various corrections can differ from the low-temperature ordering, not only due to the temperature dependence of the h_k functions but also because those corrections involve also functions of ratio ρ/ρ^* which depends on both temperature and density as shown by formula (26). For instance, the corrections associated with h_2 describing molecular formation and atom-atom interactions, will dominate in a sufficiently dense atomic phase, despite the fact that function h_2 is much smaller than h_1 (see Sec. V A).

V. COMPARISONS TO OPAL TABLES AND PIMC DATA

We compute numerically the various corrections to the ideal Saha equation of state that appear in the SLT expansion of the pressure [Eq. (25)] and of the internal energy [Eq. (32)] and compare the predictions to the most accurate current tabulations of those thermodynamical functions. The present calculations correct[2] and complement the initial results for the pressure published in Ref. [54].

TABLE II. Numerical values of functions $h_k(\beta)$ ($k = 1,2,3,4$) at different temperatures.

T (K)	$h_1(\beta)$	$h_2(\beta)$	$h_3(\beta)$	$h_4(\beta)$
2000	1.46×10^{-16}	2.89×10^{-28}	3.99×10^{-26}	1.00×10^{-31}
6000	1.70×10^{-5}	2.73×10^{-12}	6.08×10^{-9}	3.01×10^{-12}
10 000	2.23×10^{-3}	7.40×10^{-9}	2.11×10^{-5}	4.94×10^{-8}
20 000	6.84×10^{-2}	5.12×10^{-6}	8.09×10^{-3}	9.26×10^{-5}
30 000	1.88×10^{-1}	6.41×10^{-5}	4.24×10^{-2}	1.35×10^{-3}

A. General properties of the isotherms

We start by studying general properties of isotherms that follow from the structure of the terms in SLT expansion (25). Along a given isotherm, the various corrections to Saha pressure depend on the ratio ρ/ρ^* where the crossover density ρ^* is kept fixed. Because of the nonlinear dependence in ρ/ρ^* of coefficients $b_k(\rho/\rho^*)$, their relative importance changes drastically from low densities $\rho \ll \rho^*$ to high densities $\rho \gg \rho^*$. For $\rho \ll \rho^*$, each $b_k(\rho/\rho^*)$ can be expanded in powers of ρ/ρ^*, as well as Saha pressure (3) itself. This leads to the well-known virial expansion of βP in powers of ρ at fixed T [9,23,44,55,56], as shown in Ref. [54]. The corresponding leading term entirely arises from Saha pressure and describes full ionization of the plasma. First correction of order $\rho^{3/2}$, entirely provided by βP_1, is the familiar Debye contribution for a classical plasma of ionized protons and electrons with density ρ. Saha pressure (3), βP_3, and βP_5 contribute to a second correction of order ρ^2, which accounts for atomic recombination as well as two-body interactions between ionized charges. Ionic contributions embedded in βP_4 are of order ρ^3, while molecular ones embedded in βP_2 are of order ρ^4, in agreement with the numbers of protons and electrons involved in the ions H_2^+ and H^- and molecule H_2.

For ρ of order ρ^*, beyond the leading contribution of Saha pressure (3), the ranking of the various corrections is essentially that of temperature-dependent functions $h_k(\beta)$. However, notice that the *a priori* first correction βP_1 vanishes at $\rho = 4\rho^*$ and becomes positive for $\rho > 4\rho^*$. Therefore, βP_1 reduces to the familiar Debye contribution $\beta P_{\text{Debye}} = -\kappa^3/(24\pi)$ only in the fully ionized region $\rho \ll \rho^*$, while its structure begins to differ in the atomic region $\rho > \rho^*$ as a subtle consequence of recombination processes. In the region close to $\rho = 4\rho^*$, the first correction to Saha pressure is then given by βP_3 as illustrated below.

For $\rho \gg \rho^*$, Saha pressure reduces to the ideal pressure of an atomic gas with density ρ since almost all charges are recombined. According to the large-ρ/ρ^* behavior of coefficients $b_k(\rho/\rho^*)$, the first correction to Saha pressure is now given by βP_2 which describes both molecular recombination and atom-atom interactions. Since it increases as ρ^2, that correction would overcome Saha pressure at sufficiently high densities. In fact, and as discussed further, this provides an upper density for the validity of the SLT expansion. Notice that while βP_4 also increases faster than $\beta P_{\text{Saha}} \sim \rho$, i.e., as $\rho^{3/2}$, all other considered corrections increase more slowly than ρ. This can be easily interpreted by noting that such corrections, namely βP_1, βP_3, and βP_5, are related to the presence of ionized protons and electrons which tend to disappear at high densities.

The previous analysis of the behavior of the pressure along a given isotherm is summarized in Table III. Similar results hold

[2]In Ref. [54], formula (9) contains a typo and the full SLT curve in Fig. 2 of Ref. [54] is incorrect due to an ill-placed parenthesis when computing the correction $k = 3$.

TABLE III. First correction to ideal Saha pressure along a low-temperature isotherm.

Density	First correction	Physical origin
$\rho \ll \rho^*$	βP_1	Debye plasma polarization
$\rho \simeq \rho^*$	βP_3	e-p interactions and excited H atoms
$\rho \gg \rho^*$	βP_2	H_2 molecules and H-H interactions

for the behavior of the internal energy per particle given by its SLT expansion (32) together with the expressions (33)–(38). In particular, at low densities, we find that the first correction to the classical thermal energy $3kT$ of the fully ionized plasma is indeed the Debye contribution which arises entirely from u_1. For densities $\rho \gg \rho^*$, u_2 becomes the leading correction to $u_{\rm Saha}$, since it increases as ρ while u_4 grows only as $\rho^{1/2}$, u_3 tends to a constant, and both u_1 and u_5 vanish. If we replace $h_2'(\beta)$ by its low-temperature form $(3E_{\rm H} - E_{\rm H_2})h_2(\beta)$, while we introduce the molar fraction of molecules H_2 defined by $x_{\rm H_2}^{\rm id} = \rho_{\rm H_2}^{\rm id}/\rho$, then the sum of leading and subleading contributions in Eq. (32) can be rewritten as

$$\left(x_{\rm at} + x_{\rm H_2}^{\rm id}\right)\frac{3kT}{2} + x_{\rm at}E_{\rm H} + x_{\rm H_2}^{\rm id}E_{\rm H_2}, \tag{55}$$

where the molar fraction $x_{\rm at}$ of atoms H accounts for the partial recombination of protons and electrons into molecules H_2, i.e., $x_{\rm at} = x_{\rm at}^{\rm id} - 2x_{\rm H_2}^{\rm id}$. Expression (55) shows that, for $kT \ll |E_{\rm H}|$ and $\rho \gg \rho^*$, the system reduces to an ideal mixture, made of a small fraction of molecules H_2 diluted in a gas of atoms H, in their molecular and atomic ground states, respectively.

B. Isotherms at a few thousands kelvins

Because of the relatively large value of temperature scale $|E_{\rm H}|/k \simeq 150\,000$ K and of the occurrence of exponentially decaying factors, crossover density ρ^* is extremely small below a few thousand kelvins. For instance, at $T = 300$ K, we find $\rho^* \simeq 3.4 \times 10^{-204}{\rm m}^{-3}$, which corresponds to tremendously diluted conditions that are not physically accessible. This means that a stable partially ionized atomic phase, which exists when ρ is of the order of ρ^*, cannot be realized in practice for hydrogen at such low temperatures. For instance, under the standard conditions of the Earth's atmosphere, density $\rho \simeq 10^{26}{\rm m}^{-3}$ is so large with respect to ρ^* that SLT expansion breaks down, due to correction βP_2 being too large, in agreement with the emergence of molecules H_2 as the most important species. Even at $T = 2000$ K, $\rho^* = 6.1 \times 10^{-9}{\rm m}^{-3}$ still corresponds to quite diluted conditions. Interesting physical systems with similar temperatures in the range $1000{\rm K} < T < 2000{\rm K}$ are the atmospheres of brown dwarfs. The corresponding densities lie in the range $10^{25}{\rm m}^{-3} < \rho < 10^{27}{\rm m}^{-3}$, so they are too large compared to the corresponding ρ^*'s to use SLT expansions. In fact, as for Earth's atmosphere, hydrogen is essentially recombined into molecules. Thus, we will not consider isotherms below $T = 2000$ K within SLT expansions, because the corresponding density ranges of validity do not correspond to known physical systems of interest. We note that the standard virial expansion cannot provide as well any useful information on the hydrogen gas when $T < 2000$ K, for the very same reason that the fully ionized phase is not thermodynamically stable at low temperatures for physically accessible densities.

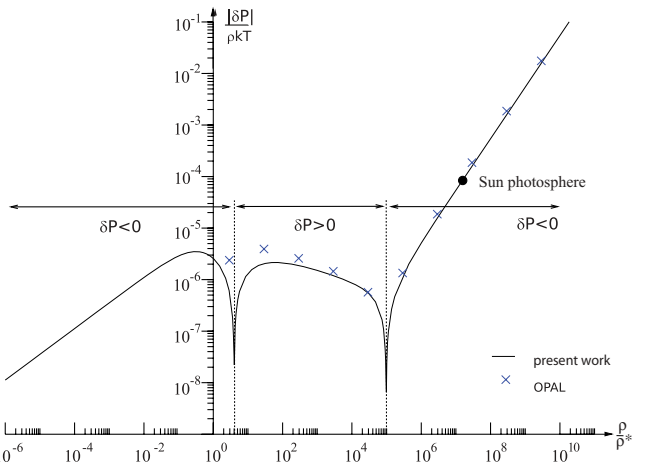

FIG. 4. (Color online) Logarithmic plot of deviations to Saha pressure for pure hydrogen along isotherm $T = 6000$ K ($\rho^* = 2.12 \times 10^{15}$ m^{-3}). Crosses correspond to tabulated points of the OPAL equation of state [1] (with corrected ground-state energy [34]).

When T increases up to a few thousands kelvins, the atomic crossover density ρ^* reaches higher values which are encountered in some systems. For fixing ideas, we consider isotherm $T = 6000$ K, which is typical of the Sun's photosphere and for which $\rho^* \simeq 2.12 \times 10^{15}{\rm m}^{-3}$. In Fig. 4, we plot deviation $\delta P = P - P_{\rm Saha}$ along that isotherm in the range $10^9{\rm m}^{-3} < \rho < 10^{27}{\rm m}^{-3}$, where δP does not exceed a few percentages of $P_{\rm Saha}$. When $\rho/\rho^* \leqslant 10^5$, the dominant contribution is due to the polarization of the plasma around ionized charges, embedded in correction P_1. For $\rho/\rho^* \leqslant 10^{-2}$, that contribution is negative and reduces to the familiar Debye expression $-\kappa^3/(24\pi)$ that appears in the virial expansion. At $\rho/\rho^* = 4$, correction P_1 changes sign, as seen on expression (27) for coefficient $b_1(\rho/\rho^*)$. The plasma-polarization correction thus is not given at high densities by the Debye formula with a modified Debye length computed with the density of ionized charges, as it could naively be expected in a phenomenological approach. At densities $\rho/\rho^* \geqslant 10^5$, molecular contributions embedded in term P_2 become the most important correction, as expected at high densities. Since the formation of molecules reduces the pressure, δP then becomes negative again. When $\rho/\rho^* \geqslant 10^{11}$, the SLT expansion fails to converge because molecular recombination can no longer be treated perturbatively.

Contributions of the first excited atomic state, embedded in correction P_3, and contributions of the ions H_2^+ and H^- embedded in P_4, are essentially negligible along the whole isotherm. For completeness, we mention that it is only near the special density $4\rho^*$ that P_3 turns out to provide the dominant correction, while P_4 is the dominant correction near the density $10^5\rho^*$ where corrections P_1 and P_2 compensate each other and where P_3 is negligible since there are almost no ionized charges. At these special densities, the deviation to the Saha pressure is about 10^{-9}.

We can compare our results to those of the OPAL tables [1], which are shown as crosses in Fig. 4. A very good agreement is found for densities $\rho/\rho^* > 10^4$. At lower densities, the

TABLE IV. Pressure at typical temperature and density of Sun photosphere.

Pressure	
$\beta P_{\rm Saha}/\rho$	$1 + 1.70 \times 10^{-4}$
$\beta P_1/\rho$	1.04×10^{-7}
$\beta P_2/\rho$	-3.79×10^{-4}
$\beta P_3/\rho$	-1.03×10^{-12}
$\beta P_4/\rho$	-2.36×10^{-8}
$\beta P_5/\rho$	-2.44×10^{-14}

discrepancies are certainly due to the fact that extracting a deviation to Saha pressure from the OPAL tables is a difficult task when the deviation is of the order of 10^{-6}. Indeed, the values in the OPAL tables are given with at most six digits, and a slight difference in the values of the fundamental constants, like in the ground-state energy $E_{\rm H}$, can induce a small variation of the Saha pressure $P_{\rm Saha}$ that is comparable to the deviation $\delta P = P - P_{\rm Saha}$ itself.

A change of sign of δP is observed in the OPAL EOS around density $\rho/\rho^* \simeq 10^5$ at 6 000 K, in agreement with our SLT EOS: This sign change is induced by negative contributions in P_2 associated with molecular recombination overcoming the plasma polarization correction P_1. Notice that the nontrivial variations of δP with two sign changes are brought to light by simple physical interpretations within our approach. At the point with density $\rho \simeq 1.47 \times 10^{23}{\rm m}^{-3}$, typical of the Sun's photosphere shown in Fig. 4, electrons and protons are almost fully recombined into hydrogen atoms since $\rho \gg \rho^*$, and the various corrections to Saha pressure, which is itself close to $P_{\rm at}^{\rm (id)}$, are given in Table IV. The full pressure is below $P_{\rm at}^{\rm (id)}$ because of molecular recombination. Moreover, contributions of ions $H_2{}^+$ and H^- are still smaller than the positive polarization contribution due to the ionized protons and electrons despite the fact that their dilution is quite large. Such subtle effects cannot be anticipated nor accurately described with phenomenological approaches.

C. Isotherms between ten and thirty thousands kelvins

We consider various isotherms above $T = 10\,000$ K up to $T = 30\,000$ K. The corresponding δP's are plotted in Fig. 5, while the respective values of ρ^* are given in Table V. The OPAL values of δP are shown, moreover, on the plots with symbols. As discovered in Ref. [34], the OPAL tables were computed using the value $E_{\rm H} = 1{\rm Ry} \simeq -13.60569$ eV, corresponding to an infinitely heavy nucleus, instead of the correct value, $E_{\rm H} = -me^4/(2\hbar^2) \simeq -13.59829$ eV. That inaccuracy in $E_{\rm H}$ induces variations of the Saha pressure that can be larger by an order of magnitude than the deviation δP itself for state points in the crossover region between the ionized and atomic phases. The OPAL deviations δP shown in all figures of the present paper were determined by subtracting from the OPAL values the ideal pressure $P_{\rm Saha}$ computed with $E_{\rm H} = 1\,{\rm Ry}$.

At the low temperatures 10 000 K and 15 000 K, we find excellent agreement between our analytical SLT EOS and the tabulated OPAL EOS in the considered density range. A small discrepancy is observed only for the last highest-density point

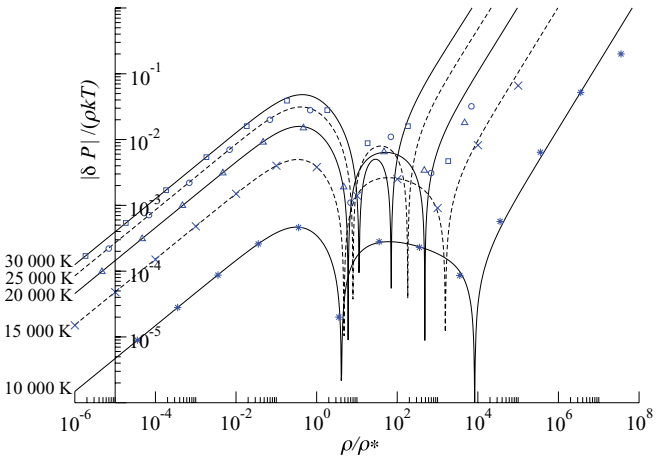

FIG. 5. (Color online) Logarithmic plots of deviations to Saha pressure along isotherms from 10 000 K up to 30 000 K according to the SLT EOS (solid and dashed lines) and to the tabulated OPAL EOS (symbols).

on each of these two curves. This discrepancy at high density (massic density 0.1 g/cm^3) and low temperatures is due to the fact that the system is close to being in a molecular phase.

At low densities, $\rho/\rho^* < 1$, the agreement between both equations of state is also excellent, even at rather high temperatures. We note that the deviation δP is dominated in that region by the Debye plasma polarization correction P_1. Although that correction changes sign at $\rho/\rho^* = 4$, deviation δP changes sign, for isotherms with $T > 10\,000$ K, at a density ρ/ρ^* slightly higher than 4 because of negative contributions arising from correction P_3, which describes excited atoms and charge-charge interactions.

We observe, in Fig. 5, discrepancies in region $\rho/\rho^* \simeq 10^2$ and $T \geqslant 20\,000$ K. Those discrepancies are due to the negative corrections P_2 and P_4, which shrink more strongly, in our calculations, the region where deviation δP is positive than in the OPAL EOS. We note that those corrections may be somewhat overestimated since we computed in the present work an approximation to functions h_2 and h_4 in which only molecular and ionic bound-state contributions are kept. The discarded truncation terms in h_2 can provide positive contributions at high temperatures, which describe in particular atom-atom interactions. An accurate calculation of functions h_2 and h_4 at temperatures higher than 20 000 K is needed to provide fully reliable results at such temperatures and densities. Tests have shown that the OPAL deviations δP around $\rho/\rho^* \simeq 10^2$ are in fact fully explained by retaining solely the Debye plasma polarization effect P_1.

TABLE V. Atomic recombination density ρ^* in m^{-3} and in g/cm^3 at various temperatures.

T (K)	$\rho^*({\rm m}^{-3})$	$\rho^*({\rm g/cm}^3)$
10 000	1.69×10^{20}	2.83×10^{-10}
15 000	5.98×10^{22}	1.00×10^{-7}
20 000	1.28×10^{24}	2.14×10^{-6}
25 000	8.65×10^{24}	1.54×10^{-5}
30 000	3.26×10^{25}	5.45×10^{-5}

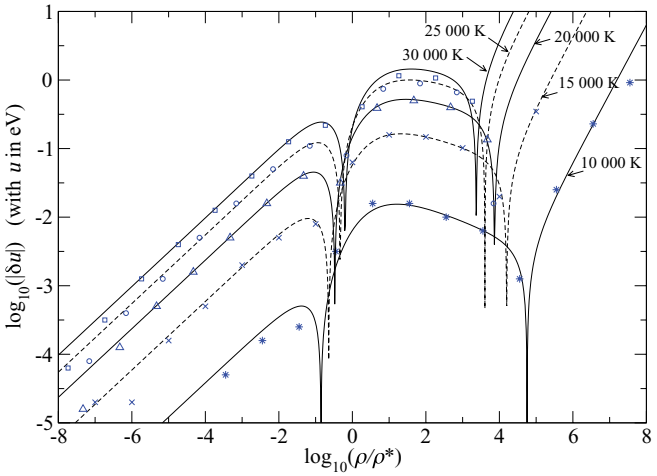

FIG. 6. (Color online) Deviations to Saha internal energy for isotherms between 10 000 K and 30 000 K according to the SLT EOS (solid and dashed lines). Points of the (corrected) OPAL EOS are shown by symbols (up to density 0.1 g/cm^3).

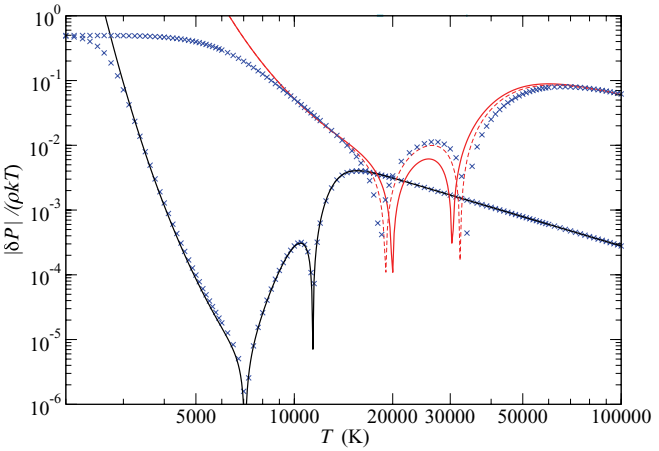

FIG. 7. (Color online) Deviations to Saha pressure along isochores 10^{-8} g/cm^3 (black line) and 10^{-3} g/cm^3 [red (light gray) line] according to the SLT EOS. Crosses correspond to values of the (corrected) OPAL EOS. The red (light gray) dashed line shows the effect of neglecting term P_4 in the SLT EOS.

Deviations $\delta u = u - u_{\rm Saha}$ of the internal energy per proton are shown along several isotherms in Fig. 6. The variations of δu at temperatures up to 10 000 K are fully controlled by the two terms u_1 and u_2. At low densities ($\rho/\rho^* \ll 1$), the plasma polarization term u_1 is dominant and negative. That correction changes sign when the condition

$$\frac{\rho}{\rho^*} = 4\epsilon\,\frac{1+\epsilon}{(1-\epsilon)^2}, \qquad \epsilon = \frac{kT}{2|E_H|} \tag{56}$$

is met, as can be seen from Eq. (34). At high densities ($\rho/\rho^* \simeq 10^4$), δu becomes negative again because the term u_2 becomes dominant and the formation of molecules indeed lowers the energy. When $T > 10\,000$ K, term u_3 comes into the game and has the effect of enlarging the domain where the deviations δu are positive, similarly to the case of the pressure deviations δP.

D. Low-density isochores

A plot of pressure deviations δP along two low-density isochores is displayed in Fig. 7 for temperatures between 2000 K and 100 000 K. The predictions of the OPAL tables, which are available for many temperature points, are also shown in those plots. At very low densities (isochore 10^{-8} g/cm^3), our calculations agree very well with the OPAL tables. When the temperature is high, the system is fully ionized and the dominant correction to Saha pressure arises from the Debye plasma polarization correction P_1, which behaves as $-\kappa^3/(24\pi) \propto T^{-3/2}$ when $T \to \infty$. On decreasing the temperature, correction P_1, and, hence, also δP, changes sign when the condition $\rho/\rho^* = 4$ is met. The deviation δP displays a second change of sign at a lower temperature, because the correction P_2 becomes dominant due to the formation of hydrogen molecules in the system. That correction P_2 grows quickly when the temperature is further lowered, and a point is reached where P_2 is no longer a small correction. This signals the formation of the molecular phase, which is outside the scope of the present calculations. Since the pressure of the ideal molecular gas is $\rho kT/2$ and that of the ideal atomic gas is ρkT, the pressure deviation $|P - P_{\rm Saha}|/(\rho kT)$ should tend to 0.5 at low temperatures and low densities, as is indeed observed for the OPAL deviations in Fig. 7.

Along isochore 10^{-3} g/cm^3 shown in Fig. 7, we can observe some discrepancies between our predictions for the deviations δP and those of the OPAL tables. When $T < 10\,000$ K, the differences are due to the formation of the molecular phase. In region $20\,000\text{K} < T < 30\,000$ K, deviation δP is positive and is somewhat larger in the OPAL tables than predicted by the SLT EOS. In that region, deviation δP is the result of the sum of the first four SLT terms, with P_2 and P_4 partially compensating P_1 and P_3. While the latter two terms are known exactly, the former two terms are currently estimated in our calculations by keeping only molecular and ionic bound states (see Sec. IV B). Not surprisingly, accurate calculations of the corresponding functions h_2 and h_4 in the temperature range 20 000–70 000 K, are required for a fully reliable description. When $T \geqslant 80\,000$ K, the SLT and OPAL predictions coincide. At such high temperatures, the deviation δP is due to the sum of the SLT terms P_1, P_3, and P_5 associated with ionized protons and electrons, and it reduces to the predictions of the standard virial expansion.

A low-density isochore of the internal energy is shown in Fig. 8, where the SLT EOS is compared to other equations of state. At high temperatures, the system is fully ionized and the variations of the internal energy per proton are mainly controlled by the average thermal kinetic energy $3kT/2$ of the particles (dot-dashed line). When the temperature is reduced to 10 000 K, a sharp drop of the internal energy is observed due to the formation of the atomic phase. Reducing further the temperature, a second drop in the potential energy occurs when the molecular phase is formed. Since the SLT EOS accounts perturbatively for all deviations to the ideal Saha equation of state that describes the transition between the ionized and the atomic phase, its validity domain is limited at low temperature by the formation of the molecular phase, which is a nonperturbative effect (see deviations at low temperatures in

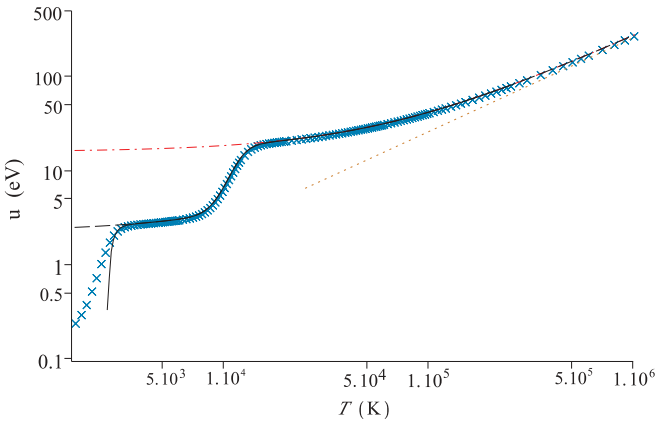

FIG. 8. (Color online) Internal energy per proton along isochore 10^{-8} g/cm^3 according to the SLT EOS (black line), OPAL EOS (crosses), and Saha EOS (dashed line). For the difference between the two former and the latter curves, see Fig. 9. All energies are shifted upwards by $|E_{H_2}|/2$. The plot shows also curves $|E_{H_2}|/2 + 3kT$ (red dot-dashed line) and $3kT$ (dotted line).

Fig. 8). On the scale of Fig. 8, the deviations $\delta u = u - u_{\rm Saha}$ between the SLT EOS or the OPAL EOS, and the ideal Saha values are almost indiscernible. Those deviations are shown in Fig. 9 for two isochores, 10^{-8} and 10^{-3} g/cm^3. The agreement on deviations δu between our analytical calculations and the OPAL tables is impressively good. As in the case of the pressure isotherms (see Fig. 5), δu changes sign twice: once in the ionized-atomic transition, when condition (56) is met, and once in the atomic-molecular crossover region. The only significant disagreement between the SLT and OPAL EOS along the very low density isochore (10^{-8} g/cm^3) occurs at low temperatures due to the formation of the molecular phase, where the OPAL deviation δu tends to the difference in energy per proton between the atomic and the molecular phase $[\log_{10}(E_{H_2}/2 - E_H) \simeq 0.35]$. Along isochore 10^{-3} g/cm^3, rather small differences are observed only near the two sign changes of δu, similarly to the deviations δP along the same

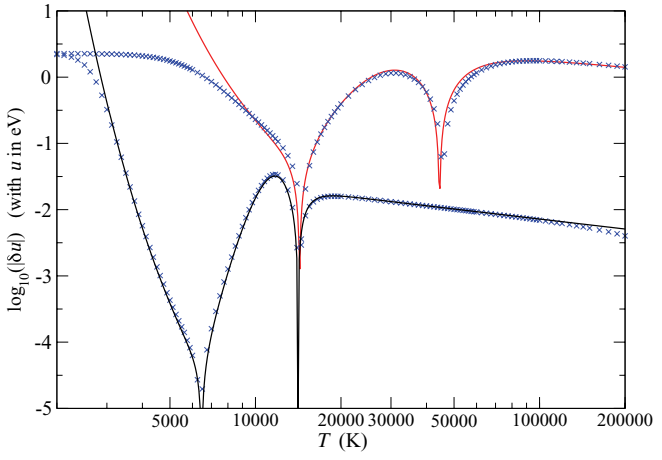

FIG. 9. (Color online) Deviations to Saha internal energy for isochores 10^{-8} g/cm^3 (black line) and 10^{-3} g/cm^3 [red (light gray) line] according to the SLT EOS. Crosses denote tabulated points of the (corrected) OPAL EOS.

isochore. Term u_5 contributes sensitively to δu only when $T \geqslant 30\,000$ K.

E. Comparison to PIMC data

Results of quantum path integral Monte Carlo (PIMC) simulations of a dilute e-p gas are available at six densities between 10^{-3} g/cm^3 and 0.15 g/cm^3 and eight temperatures between 5000 K and 250 000 K [4] (see state points in Fig. 12). Very low densities, such as 10^{-6} g/cm^3 as in the Sun photosphere, are not within reach of PIMC simulations because sufficient statistics cannot be collected in very diluted conditions. Fortunately, the SLT expansion converges quickly at such low densities, and it has been shown in the previous section that the predictions of the SLT EOS coincide in this regime with those of the (corrected) OPAL tables, if we exclude the molecular phase which is outside the validity domain of the SLT expansion.

Comparison of our results with the PIMC data is instructive along the moderate density isochore 10^{-3} g/cm^3; see Fig. 10. The decrease of the pressure as the temperature is lowered is shown in Fig. 10(a), with P varying from $2\rho kT$ at high temperature (fully ionized gas) to ρkT (atomic gas at around 15 000 K), and eventually down to $\rho kT/2$ (molecular phase). A small plateau corresponding to the atomic phase can also be identified in Fig. 10(b) for the internal energy, though it is much less visible than on isochore 10^{-8} g/cm^3 (see Fig. 8). The deviations δP and δu from the ideal Saha values are shown in Figs. 10(a′) and 10(b′). The various sign changes of these deviations predicted by the SLT formulas can indeed be observed in the simulations. The uncertainties of the simulation data at temperatures $T \leqslant 15\,000$ K are quite large, especially in the case of the pressure. Notice that $\delta P/(\rho kT)$ tends trivially to $-1/2$ in a dilute molecular phase, so the simulation data do not contain much information in that regime. In the crossover region between the atomic phase and the fully ionized phase, the agreement on δP and δu between the simulation data and the SLT and OPAL equations of state is rather good. In the temperature range 10 000−25 000 K, the predictions of the SLT EOS are within the error bars of the PIMC results. At very high temperatures, $T > 100\,000$ K, the PIMC results for the energy deviation δu do not agree fully with the SLT nor the OPAL EOS. The uncertainties in the simulation results are maybe underestimated. When $T = 62\,500$ K, and to a lesser extent when $T = 31\,250$ K, the OPAL EOS agrees slightly better with the PIMC data than the SLT EOS. This might be due to our inaccurate description of functions h_2 and h_4 for such temperatures.

In Fig. 11, we compare our results along a denser isochore at massic density 0.0125 g/cm^3 (for which $r_s = a/a_B = 6$), where significant differences between the predictions of the three approaches (SLT EOS, OPAL EOS, and PIMC simulations) can be observed, especially in the case of the pressure deviations. Disregarding the molecular phase at low temperatures, deviations δP and δu remain small (less than 10%) along this isochore, so the SLT expansion should still apply. Since the OPAL EOS agrees quite well with the PIMC data for the energy deviations δu and the OPAL EOS is thermodynamically consistent, the disagreement on the OPAL pressures with the PIMC data when $T \leqslant 30\,000$ K, i.e., in the

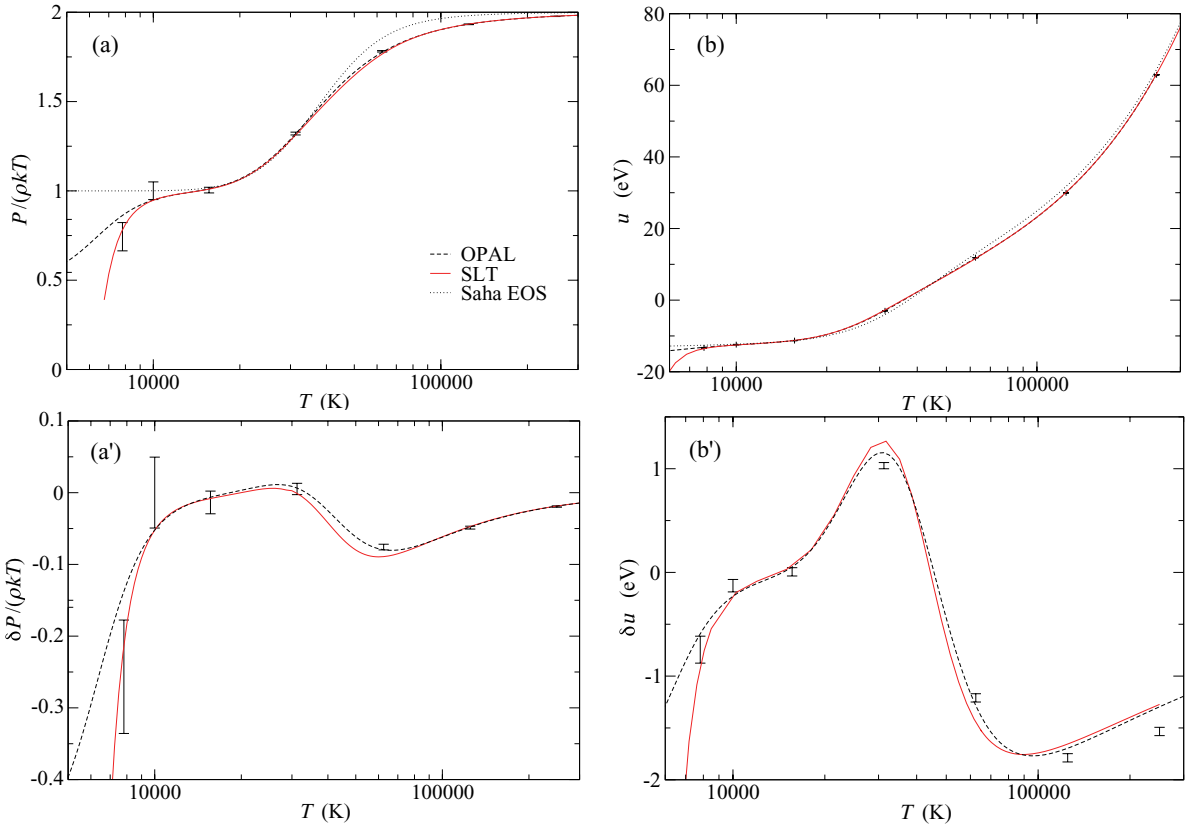

FIG. 10. (Color online) Pressure (a) and internal energy (b) per electron-proton pair as a function of temperature along isochore 10^{-3} g/cm^3, according to SLT EOS [red (light gray) line], OPAL EOS (dashed line), and ideal Saha EOS (dotted line). Points with error bars are simulation results of Ref. [4]. Plots (a′) and (b′) show deviations to the ideal Saha values along the isochore.

crossover region between the atomic and the molecular phase, indicates probably that the errors on the PIMC pressures are underestimated. Some disagreement between the OPAL (and SLT) equations of state and the PIMC results is also observed at 31 250 K and at high temperatures for $T \geqslant 100\,000$ K. As for the above lower-density isochore, some discrepancies between the SLT EOS and the other data might be due to inaccuracies in the calculation of functions $h_2(T)$ and $h_4(T)$ for temperatures above 30 000 K.

F. Validity domain

As exemplified in the previous sections, truncation of the SLT expansion (25) at $k = 5$ gives accurate results as long as the corresponding deviations $\delta P = \sum_{k=1}^{5} P_k$ or $\delta u = \sum_{k=1}^{5} u_k$ remain small compared to their ideal Saha value. The validity of the SLT expansion is limited at high densities along an isotherm, respectively at low temperatures along an isochore, by the formation of the molecular phase, where βP_2 then becomes larger than $P_{\rm Saha}$ itself. We can estimate the borderline of the validity domain by introducing the empirical criterion $|\delta P(T_{\rm v},\rho)| = P_{\rm Saha}/10$. At high densities, or low temperatures, $\rho \gg \rho^*$ so P_2 becomes the leading correction in δP. Criterion $|P_2|/P_{\rm Saha} = 0.1$ then gives

$$\rho_{\rm c}(T) = \frac{\rho^*(T)}{20|h_2(T)|} \tag{57}$$

as a borderline for the validity domain in the (ρ,T) plane. If the temperature is low, function $h_2(T)$ behaves as

$$h_2(T) \sim \frac{1}{64}\left(\frac{2m}{M}\right)^{3/2} \exp[(3E_{\rm H} - E_{\rm H_2})/(kT)], \tag{58}$$

and $\rho_c(T)$ reduces to a straight line in the $(\log\rho,\ \beta)$ plane (see Fig. 12). The curve $\rho_c(T)$ defines quite precisely the borderline of the validity domain in a large part of the phase diagram, as checked by the comparison with the data of the PIMC simulations. In particular, this is illustrated by the plots in Sec. IV E and the state points denoted by crosses in Fig. 12. At a given density, the SLT expansion converges only for temperatures that are sufficiently high to avoid the formation of the molecular phase. Some of the lower-temperature state points in the PIMC simulations are, for instance, outside of the validity domain of the SLT expansion, while others, like those to the left of line $\rho_c(T)$ in Fig. 12, are within the validity domain. When the density increases, the minimum temperature required for the SLT expansion to converge also increases. At density 0.1 g/cm^3, the temperature must be higher than 30 000 K. Since the exact behavior of $h_2(T)$ above 30 000 K is currently not available, the precise position of the borderline of the validity domain in the region of high densities and temperatures is yet not fully known.

The crossover density $\rho^*(T)$ [Eq. (2)] between the fully ionized and the atomic phase is also shown in Fig 12. That line gives essentially the borderline of the validity domain

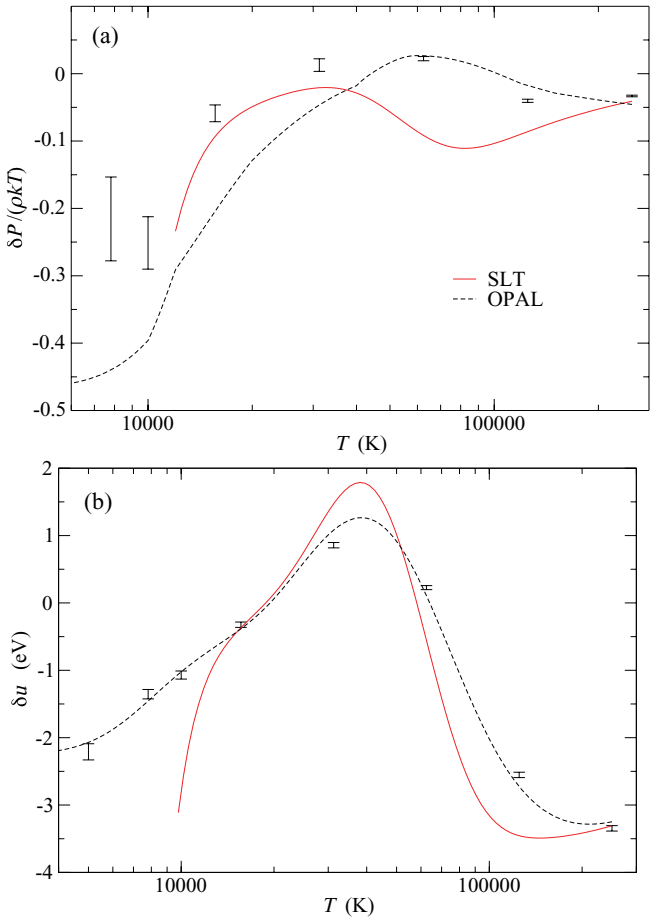

FIG. 11. (Color online) Deviations (with respect to ideal Saha values) of pressure (a) and internal energy per electron-proton pair (b) as a function of temperature along isochore 0.0125 g/cm^3, according to the SLT EOS [red (light gray) line] and OPAL EOS (dashed line). Points are simulation results of Ref. [4].

of the standard virial expansion, which holds only in the weakly coupled ($\Gamma \ll 1$) fully ionized phase. The dashed line in Fig. 12 shows state points where the coupling parameter $\Gamma = \beta^2/a$ is equal to 0.5. That line lies quite close to $\rho^*(T)$. In the narrow strip at high densities and temperatures between the lines $\Gamma = 0.5$ and $\rho^*(T)$, the SLT expansion is expected to converge only slowly because Γ is close to 1 ($\Gamma \leqslant 0.7$ in that region).

Figure 12 shows that the SLT expansion provides an accurate analytical knowledge of the thermodynamics of the quantum e-p gas in a rather large range of densities and temperatures that includes the fully ionized phase ($\rho \ll \rho^*$), the partially ionized phase ($\rho \sim \rho^*$), and the atomic phase ($\rho^* \ll \rho < \rho_c$).

VI. CONCLUSIONS

In this work, we extend the exact analytical knowledge on the thermodynamics of hydrogen at low densities by deriving the first five terms in the SLT expansion of the internal energy [Eq. (32)], a result that complements the corresponding expansions for the pressure [Eq. (25)] and the chemical potential [Eq. (20)]. Similar expansions for

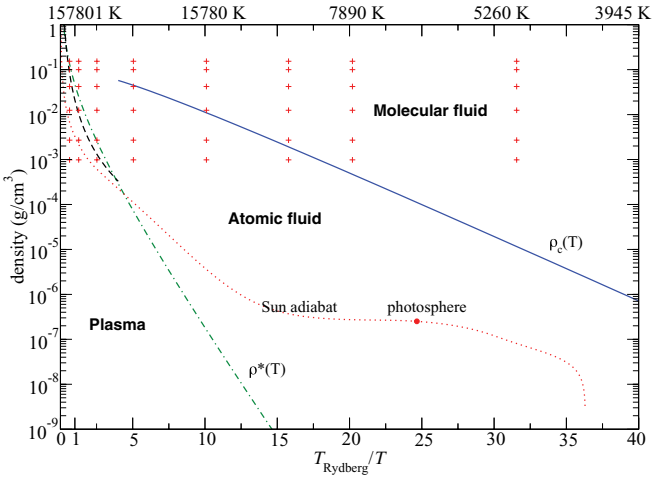

FIG. 12. (Color online) Phase diagram of a pure hydrogen gas at low densities. The crosses denote state points where simulation results are available [4]. The crossover density $\rho^*(T)$ between the plasma and the atomic phase (dot-dashed line) gives essentially the borderline of the validity domain of the standard virial expansion, which applies only in the plasma phase. The dashed line corresponds to a plasma coupling parameter $\Gamma = 0.5$. The SLT expansion is valid in both the plasma and atomic phases, up to the solid (blue) line $\rho_c(T)$ [Eq. (57)], which locates the crossover to the molecular phase. The state point of the Sun photosphere and the track of the Sun adiabat (dotted line) are also shown.

any thermodynamical quantity can be easily derived without any loss of thermodynamic consistency. We performed also extensive numerical calculations of isotherms and isochores and compared in detail the predictions of the SLT formulas with the numerical OPAL EOS and data of PIMC simulations. Our analytical SLT formulas for the deviations to the ideal Saha law can be evaluated numerically very easily and quickly. As applying the SLT EOS is straightforward, no extensive tabulation, with the associated loss of accuracy due to interpolation, is required. A plot and a tabulation of the functions $h_k(\beta)$ ($k = 1,2,3,4$) have been provided as guide to help the user in applying numerically our formulas.

We emphasize the following points:

(1) The exact SLT expansion overcomes the restriction $\rho \ll \rho^*(T)$ of the standard virial expansion and has a validity domain that extends up to the density $\rho_c(T)$ in the atomic phase (see Fig. 12).

(2) At low densities ($\rho < 10^{-5}$ g/cm^3), excellent agreement is found between the predictions of the SLT EOS for the pressure and the internal energy and the values in the OPAL tables for pure hydrogen. Notice that if the density is very low, the OPAL tables need to be corrected as explained in Ref. [50]. As several important ingredients in the OPAL EOS, which is available only in the form of precomputed tables, are unknown, attempts have been made to emulate this equation of state [57]. It is very satisfactory to see that the OPAL EOS for pure hydrogen can be fully reproduced at low densities by our simple analytical formulas. Furthermore, the physical content of the various corrections of interest is enlightening, as well as the subtle cancellations between some contributions. No PIMC simulation results are available at such low densities because the statistics becomes poor.

(3) At higher densities, some small discrepancies can be observed among the SLT EOS, the OPAL EOS, and the simulation results. We plotted the pressure deviations $\delta P = P - P_{\rm Saha}$ and the energy deviations $\delta u = u - u_{\rm Saha}$ to the ideal Saha law to extract the variations of those thermodynamical quantities that are due to nonideality. Those deviations δP and δu show two sign changes, which are also seen in the simulation data and which are fully explained by our analytical formulas. For densities up to 10^{-3} g/cm^3 and temperatures up to 30 000 K, the SLT EOS and the OPAL EOS are both within the error bars of the PIMC simulations.

(4) At densities around 10^{-2} g/cm^3 and above, and for temperatures above 30 000 K, there are some discrepancies between the deviations, especially δP, calculated from the PIMC data and those of the SLT and OPAL EOS. In that range of temperatures, our present approximate expressions for $h_2(\beta)$ and $h_4(\beta)$ are not reliable. Better estimations of those functions, based on a numerical evaluation of path integral formulas for the internal partition functions $Z(2,2)$, $Z(2,1)$, and $Z(1,2)$, would provide an interesting improvement of our calculations, in particular in the region $\rho \geqslant 10^{-3}$ g/cm^3 and $T \geqslant 30\,000$ K.

As shown in Ref. [34], expansion (13) of particle density in terms of chemical potential should remain valid in the molecular regime, i.e., for $\rho \geqslant \rho_c$, provided the density is not too high. The accurate knowledge of $Z(2,2)$, $Z(2,1)$, and $Z(1,2)$ within numerical path integration, together with a numerical inversion of Eq. (13), should, therefore, provide a precise description of the crossover transition from the atomic gas to the molecular gas, much beyond the level of accuracy of current calculations, including PIMC simulations [34]. The accurate calculations of $Z(2,2)$, $Z(2,1)$, and $Z(1,2)$ via numerical path integrations would include in particular the contributions of atom-atom interactions. Such contributions are not easy to determine within simple modelizations because of the difficulty, intrinsic to quantum mechanics, in separating them from purely molecular contributions.[3] The accurate knowledge of $Z(2,2)$, $Z(2,1)$, and $Z(1,2)$ might also be useful for improving chemical approaches, like the Saumon-Chabrier theory [58], the MHD model [25], or the SAHA-S model [59].

The track of the Sun adiabat [60] stays well within the validity domain of the SLT expansion. The presents results are, therefore, of interest for astrophysics, where a very accurate EOS is needed, for instance, to interpret recent seismology measurements in the Sun [7,60]. The SLT expansion of other thermodynamical properties, such the adiabatic exponent and the sound speed, can be derived along similar lines. For real applications to helioseismology, the present calculations must be generalized to the case of a hydrogen-helium mixture within similar tools, an *a priori* feasible task. The contributions of other heavier elements might be determined within simple ideal approximations since their dilution is very high. Notice that relativistic effects associated with the electrons should be also incorporated as discussed in Refs. [61,62].

[3]Notice that in Ref. [54], we proposed a simple approximation for those contributions, which needs to be improved for tackling regimes with $T > 30\,000$ K.

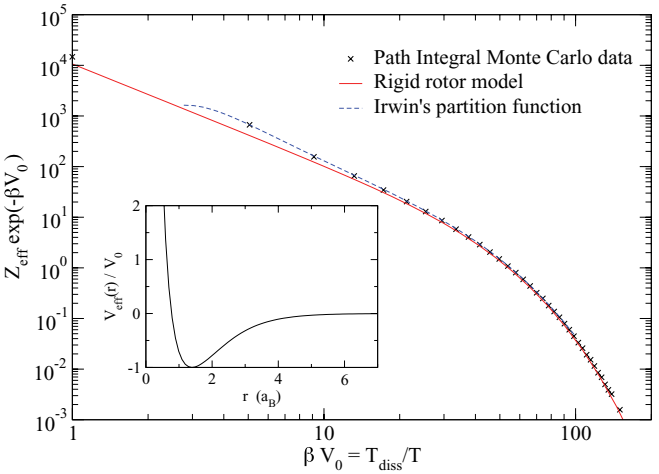

FIG. 13. (Color online) The truncated trace $Z_{\rm eff} = {\rm Tr}[\exp(-\beta H_{\rm eff}) - \exp(-\beta H_0)]$ for a quantum particle in the effective proton-proton potential of the H_2 molecule (shown in the inset), as obtained from a numerically exact path integral Monte Carlo calculation (crosses), from the rigid rotor approximation (A4) (solid line) and from Irwin's partition function [53] (dashed curve). The dissociation temperature of the H_2 molecule is $T_{\rm diss} = V_0/k = 55\,459$ K.

APPENDIX: A SIMPLIFIED MODEL

Let us consider a simple model which is often used for describing the H_2 molecule [63]. In that model, the two protons separated by a distance R interact *via* a potential $V_{\rm eff}(R)$ which is inferred from the electronic ground-state wave function for that fixed protonic configuration. The potential $V_{\rm eff}(R)$ is repulsive at short distances, attractive at large distances, and minimum at $R = R_0$ with $V_{\rm eff}(R_0) < 0$. A plot of that potential, obtained by fitting the data of Ref. [63] to the formula

$$V_{\rm eff}(R) = (1 + aR + bR^2 + cR^3)\frac{\exp(-R/d_A)}{R} - \frac{6.5}{d_B^6 + R^6} \tag{A1}$$

is shown in the inset of Fig. 13, while the values of the fitted coefficients are given in Table VI. Equation (A1) is written in atomic units: lengths are measured in units of the Bohr radius and energies in units of the Hartree energy (1 $E_{\rm h}$ = 2 Ry). The zero of energy corresponds here to the state with two hydrogen atoms infinitely far apart. The minimum of the potential is located at $R_0 = 1.3924$ (in atomic units) with value

TABLE VI. Parameters of potential (A1) that best fit the data of Ref. [63] for the hydrogen molecule.

Coefficient	Value (in a.u.)
a	−0.52906
b	−0.60479
c	−0.37294
d_A	0.64160
d_B	2.64591

$V(R_0) = -V_0 = -0.175629$ hartree. The dissociation energy of the hydrogen molecule is $T_{\rm diss} = V_0/k = 55\,459$ K.

For our purpose, it is sufficient to consider that the protons are spinless. A proper account of the spins would lead to the usual coupling between spin and position variables, which in turn induce a different counting of ortho- and parahydrogen contributions; see, for instance, formula (50).

The Hamiltonian of the relative particle with mass $m^* = m_{\rm p}/2$ submitted to $V_{\rm eff}(R)$ reads

$$H_{\rm eff} = -\frac{\hbar^2}{2m^*}\Delta_{\mathbf{R}} + V_{\rm eff}(R). \tag{A2}$$

Within that simplified model, the analog of the contribution of $[\exp(-\beta H_{2,2}) - \exp(-\beta H_{1,1})\exp(-\beta H_{1,1})]$ to $h_2(\beta)$ is the truncated trace

$$Z_{\rm eff} = {\rm Tr}[\exp(-\beta H_{\rm eff}) - \exp(-\beta H_0)], \tag{A3}$$

where H_0 is the kinetic part of $H_{\rm eff}$.

Let $E_0 = E_{\rm H_2} - 2E_{\rm H} \simeq -0.94188\,V_0$ be the ground-state energy of $H_{\rm eff}$. Instead of determining exactly all bound-state energies of $H_{\rm eff}$ by solving the corresponding radial Schrodinger equation for various values of orbital number l, we consider the usual rigid-rotor and harmonic well approximations for describing global rotations and vibrations. Then, on the one hand, the approximation analoguous to Eq. (47) for $h_2(\beta)$ becomes

$$Z_{\rm eff} \simeq \exp(-\beta E_0)\frac{1}{1-\exp\left(-\beta\epsilon_{\rm eff}^{\rm (vib)}\right)}\sum_{l=0}^{\infty}(2l+1) \times \exp\left[-l(l+1)\beta\epsilon_{\rm eff}^{\rm (rot)}\right], \tag{A4}$$

where $\epsilon_{\rm eff}^{\rm (rot)} = kT_{\rm eff}^{\rm (rot)}$ and $\epsilon_{\rm eff}^{\rm (vib)} = kT_{\rm eff}^{\rm (vib)}$ are the rotational and vibrational quanta which can be determined respectively from R_0 and from the shape of $V_{\rm eff}(R)$ around its minimum at $R = R_0$: $T_{\rm eff}^{\rm (rot)} = 88.7$ K and $T_{\rm eff}^{\rm (vib)} = 6524$ K. On the other hand, we have performed a numerical calculation of $Z_{\rm eff}$ within path integral Monte Carlo methods applied to its Feynman-Kac path integral representation [47],

$$Z_{\rm eff} = \frac{1}{(2\pi(\lambda^*)^2)^{3/2}}\int d\mathbf{R}\int \mathcal{D}_{\rm W}(\boldsymbol{\xi}) \times\left[\exp\left[-\beta\int_0^1 ds\,V_{\rm eff}(\mathbf{R}+\lambda^*\boldsymbol{\xi}(s))\right]-1\right], \tag{A5}$$

where $\boldsymbol{\xi}(s)$ is a Brownian bridge such that $\boldsymbol{\xi}(1) = \boldsymbol{\xi}(0) = 0$, $\mathcal{D}_{\rm W}(\boldsymbol{\xi})$ is the normalized Wiener measure, and $\lambda^* = (\beta\hbar^2/m^*)^{1/2}$. At low temperatures ($T \ll T_{\rm diss}$), the truncated trace $Z_{\rm eff}$ is dominated by the contributions arising from bound states with negative energies since the corresponding contributions grow exponentially fast when $\beta \to \infty$. Figure 13 shows that the approximation (A4) (which amounts to keeping only bound-state contributions evaluated within the rigid rotor model) represents quite well the Monte Carlo values for $Z_{\rm eff}$ up to $T \simeq 30\,000$K. Thus, we can reasonably expect a similar accuracy for approximation (47). We note that Irwin's partition function [53], which accounts for rotational-vibration coupling in molecule H_2 by summing explicitly on calculated rovibrational energy levels, provides a better fit to the Monte Carlo data for this simplified model, but Irwin's partition function is available only up to 16 000 K. At high temperatures (30 000 K and above), a precise evaluation of the contributions besides those of the bound states, i.e., contributions arising from diffusive states as well as those due to the truncation terms in $h_2(\beta)$, becomes mandatory.

[1] F. J. Rogers and A. Nayfonov, Astrophys. J. **576** 1064 (2002); F. J. Rogers, F. J. Swenson, and C. A. Iglesias, *ibid.* **456**, 902 (1996).

[2] F. J. Rogers, Phys. Rev. A **10**, 2441 (1974).

[3] F. J. Rogers, Phys. Rev. A **24**, 1531 (1981); Astrophys. J. **310**, 723 (1986); in *The Equation of State in Astrophysics*, edited by G. Chabrier and E. Schatzman (Cambridge University Press, New York, 1994).

[4] B. Militzer and D. M. Ceperley, Phys. Rev. E **63**, 066404 (2001).

[5] F. J. Rogers and D. A. Young, Phys. Rev. E **56**, 5876 (1997).

[6] A. Alastuey, V. Ballenegger, F. Cornu, and Ph. A. Martin, J. Stat. Phys. **130**, 1119 (2008).

[7] W. Däppen, J. Phys. A: Math. Gen. **39**, 4441 (2006).

[8] T. Morita, Prog. Theor. Phys. **22**, 757 (1959).

[9] W. Ebeling, Ann. Phys. Leipzig **19**, 104 (1967).

[10] C. Deutsch, Phys. Lett. A **60**, 317 (1977).

[11] H. Minoo, M. M. Gombert, and C. Deutsch, Phys. Rev. A **23**, 924 (1981).

[12] H. E. DeWitt, M. Schlanges, A. Y. Sakakura, and W. D. Kraeft, Phys. Lett. A **197**, 326 (1995).

[13] D. Kremp, M. Schlanges, and W.-D. Kraeft, *Quantum Statistics of Nonideal Plasmas* (Springer, Berlin, 2005).

[14] A. Alastuey, F. Cornu, and A. Perez, Phys. Rev. E **49**, 1077 (1994).

[15] D. C. Brydges and Ph. A. Martin, J. Stat. Phys. **96**, 1163 (1999).

[16] V. Ballenegger, Ph. A. Martin, and A. Alastuey, J. Stat. Phys. **108**, 169 (2002).

[17] F. Perrot and M. W. C. Dharma-wardana, Phys. Rev. E **52**, 5352 (1995).

[18] T. J. Lenosky, S. R. Bickham, J. D. Kress, and L. A. Collins, Phys. Rev. B **61**, 1 (2000).

[19] W. Lorenzen, B. Holst, and R. Redmer, Phys. Rev. Lett. **102**, 115701 (2009).

[20] C. Pierleoni, D. M. Ceperley, B. Bernu, and W. R. Magro, Phys. Rev. Lett. **73**, 2145 (1994).

[21] A. Alastuey, V. Ballenegger, F. Cornu, and Ph. A. Martin, J. Stat. Phys. **113**, 455 (2003).

[22] A. Alastuey, F. Cornu, and A. Perez, Phys. Rev. E **51**, 1725 (1995).

[23] A. Alastuey and A. Perez, Phys. Rev. E **53**, 5714 (1996).

[24] F. Cornu, Phys. Rev. E **58**, 5268 (1998); **58**, 5293 (1998); **58**, 5322 (1998).

[25] D. Mihalas, W. Däppen, and D. Hummer, Astrophys. J. **331**, 815 (1988).

[26] A. Y. Potekhin, Phys. Plasm. **3**, 4156 (1996).

[27] G. Massacrier, A. Y. Potekhin, and G. Chabrier, Phys. Rev. E **84**, 056406 (2011).

[28] M. R. Zaghloul, Phys. Rev. E **69**, 026702 (2004).

[29] Y. V. Arkhipov, F. B. Baimbetov, and A. E. Davletov, Phys. Rev. E **83**, 016405 (2011).
[30] A. V. Filinov, V. O. Golubnychiy, M. Bonitz, W. Ebeling, and J. W. Dufty, Phys. Rev. E **70**, 046411 (2004).
[31] Y. A. Omarbakiyeva, C. Fortmann, T. S. Ramazanov, and G. Röpke, Phys. Rev. E **82**, 026407 (2010).
[32] M. Saha, Philos. Mag. **40**, 472 (1920).
[33] N. Macris and Ph. A. Martin, J. Stat. Phys. **60**, 619 (1990).
[34] A. Alastuey and V. Ballenegger, Contrib. Plasma Phys. **52**, 95 (2012).
[35] E. H. Lieb and J. Lebowitz, Adv. Math. **9**, 316 (1972).
[36] C. Fefferman, Rev. Math. Iberoamericana **1**, 1 (1985).
[37] J. G. Conlon, E. H. Lieb, and H. T. Yau, Commun. Math. Phys. **125**, 153 (1989).
[38] I. Iosilevskiy, Contrib. Plasma Phys. **49**, 713 (2009).
[39] L. Brillouin, *Les Statistiques Quantiques et leurs Applications* (Presse Univ. de France, Paris, 1930).
[40] A. I. Larkin, Sov. Phys. JETP **11**, 1363 (1960).
[41] A. Alastuey and V. Ballenegger, J. Phys. A: Math. Theor. **42**, 214031 (2009).
[42] D. Bollé, Ann. Phys. (NY) **121**, 131 (1979).
[43] D. Kremp, W. D. Kraeft and A. J. M. D. Lambert, Physica A **127**, 72 (1984).
[44] W. D. Kraeft, D. Kremp, W. Ebeling, and G. Röpke, *Quantum Statistics of Charged Particle Systems* (Plenum Press, New York, 1986).
[45] W. Ebeling, Physica **40**, 290 (1968).
[46] W.-D. Kraeft, J Phys: Conf. Ser. **11**, 131 (2005).
[47] H. Kleinert, *Path Integrals in Quantum Mechanics, Statistics, Polymer Physics and Financial Markets* (World Scientific, Singapore, 2004).
[48] B. Jancovici, Physica A **91**, 152 (1978).
[49] W. Ebeling, W. D. Kraeft, and G. Röpke, Ann. Phys. **524**, 311 (2012).
[50] V. Ballenegger, Ann. Phys. (Berlin) **524**, 103 (2012).
[51] W. Ebeling, W. D. Kraeft, and G. Röpke, Contrib. Plasma Phys. **52**, 7 (2012).
[52] L. D. Landau and E. M. Lifchitz, *Quantum Mechanics*, 3rd ed. (Pergamon Press, Oxford, 1977), Vol. 3.
[53] A. W. Irwin, Astron. Astrophys. **182**, 348 (1987).
[54] A. Alastuey and V. Ballenegger, Contrib. Plasma Phys. **50**, 46 (2010).
[55] A. Alastuey and A. Perez, Europhys. Lett. **20**, 19 (1992).
[56] T. Kahlbaum, J. Phys. IV France **10**, 455 (2000).
[57] H-H. Lin and W. Däppen, Contrib. Plasma Phys. **52**, 126 (2012).
[58] D. Saumon and G. Chabrier, Phys. Rev. A **46**, 2084 (1992).
[59] V. K. Gryaznov, S. V. Ayukov, V. A. Baturin, I. L. Iosilevskiy, A. N. Starostin, and V. E. Fortov, J. Phys. A: Math. Gen. **39**, 4459 (2006).
[60] J. Christensen-Dalsgaard *et al.*, Science **272**, 1286 (1996).
[61] V. K. Gryaznov, S. V. Ayukov, V. A. Baturin, I. L. Iosilevskiy, A. N. Starostin, and V. E. Fortov, in Equation-of-state and phase-transition issues in models of ordinary astrophysical matter, edited by V. Celebonovic, W. Däppen, and D. Gough, AIP Conf. Proc. **731**, 147 (2004).
[62] A. N. Starostin and V. C. Roerich, Plasma Sources Sci. Technol. **15**, 410 (2006).
[63] W. Kolos and L. Wolniewicz, J. Chem. Phys. **43**, 2429 (1964).